

Conformations of amphiphilic diblock star copolymers

Fabio Ganazzoli[†]

Dipartimento di Chimica, Politecnico di Milano, via L. Mancinelli 7, 20131 Milano, Italy

Yuri A. Kuznetsov[‡]

Centre for High Performance Computing Applications, University College Dublin, Belfield, Dublin 4, Ireland

Edward G. Timoshenko^{*}

Theory and Computation Group, Department of Chemistry, University College Dublin, Belfield, Dublin 4, Ireland

SUMMARY:

We study conformations assumed by single diblock star copolymers in a poor solvent by means of the Gaussian variational theory and Monte Carlo simulation in continuous space. Cases of stars with internal and external hydrophobic blocks are analysed. While in the former case the collapsed state has an obvious micellar shape, the latter case exhibits two nontrivial conformational structures. Apart from the equilibrium state of a globular hydrophobic core with hydrophilic daisy loops, one also finds here a metastable state of outstretched hydrophilic blocks with hydrophobic subglobules at their ends. Such a state appears to be rather long-lived during the kinetics of collapse of a swollen star. The plots of monomer densities and other observables computed by both techniques are found to be in good agreement with each other.

I. INTRODUCTION

Presently there is a great deal of interest in properties of amphiphilic copolymers because of the variety and extent of conformational transitions they show under a temperature or pH variation^{1,2}. For instance, as such copolymers contain both hydrophobic and hydrophilic (polar) monomers they can form monomolecular micelles with a hydrophobic core in water, as well as inverted micelles in apolar solvents. Furthermore, these systems have an interesting analogy to globular proteins in the folded state³. For a discussion of similarities between “coarse-grained” features of proteins and those of amphiphilic polymers we refer to ref.⁴.

Linear copolymers, in particular linear diblock copolymers, would aggregate under certain conditions, giving rise to a fascinating range of self-assembled supramolecular ordering in the absence of solvent^{2,5}, and therefore the main issues of study traditionally have been the critical micelle concentration and the solid state morphology. On the other hand, the possibility of forming monomolecular micelles is greatly increased by using more complicated topologies, for instance star or comb polymers⁶.

Random branching of polymers is indeed quite common, but carefully controlled polymerisation procedure allows one to obtain regular stars, which present a particularly nice object for theoretical study due to their symmetry and simplicity. Star polymers are believed to find a number of future applications for coating, as additives and possibly in drug delivery systems related to their low viscosity and other interesting properties.

The aim of the present paper is to investigate the behaviour of diblock star copolymers comprising both hydrophilic and hydrophobic monomers within the same arm in dilute solution. We shall not consider here the case of miktoarm star copolymers comprising chemically homogeneous arms made of two or more different monomers⁷.

Our study will be carried out by means of both the analytical Gaussian self-consistent theory and Monte Carlo simulation in continuous space. Such combination of techniques would permit us to assess the validity of the analytical theory, which up to now was independently developed and used by our two Groups in Milan and Dublin to investigate the behaviour of random linear copolymers, though in seemingly distinct formulations. In Appendix of this article we shall demonstrate the equivalence of these two versions of the theory by relating the free energy expressions in both. We would like to emphasise that this general analytical approach is the only one, to the best of our knowledge, which can explicitly account for the details of intramolecular conformation, thus providing more refined characteristics of

[†]E-mail: Fabio.Ganazzoli@polimi.it

[‡]Web page: <http://www.ucd.ie/chpca>; E-mail: yuri@ucd.ie

^{*}Author to whom correspondence should be addressed. Internet: <http://darkstar.ucd.ie>; E-mail: Edward.Timoshenko@ucd.ie

the polymer than simply the overall molecular size or density profile. The predicted intramolecular conformations may then be compared with those from direct computer simulations.

Computer simulations of star polymers (see e.g. refs.^{8,9} for recent reviews) have been carried out by a number of techniques, ranging from Monte Carlo methods, both on and off lattice, to Brownian Dynamics and Molecular Dynamics⁹. Most of works on block copolymer stars, however, dealt with the molten state and the supramolecular organisation under such conditions.

The only study on diblock star copolymers in dilute solutions similar to ours, as far as we are aware, was carried out by means of a lattice Monte Carlo simulation in ref.¹⁰. The latter paper appears to contain a somewhat confusing description of the adopted interactions model and its status. Judging by the actually observed star conformations, those correspond to the case in which both types of units are strongly immiscible with each other and also both tend to avoid the solvent molecules. This is not, of course, what one would really call an amphiphilic polymer, in which one type of units should “like” solvent while the other should not.

Besides, there are quite obvious limitations of the lattice model as such (see e.g. discussion in ref.¹¹), which become even more serious for a star polymer. Indeed, the core monomer on a lattice has a great difficulty to move at all due to its high coordination number (equal to the number of arms f). The resulting rejection of all attempted moves for some kind of motions is called a quasi–nonergodicity, a problem which is hard to deal with even for linear copolymers. If such a situation occurs, it practically means that the results of the simulation may no longer be trusted. A number of complicated non–local moves involving the core monomer have been suggested to alleviate this problem¹². However, such moves are not permitted in case of Dynamic Monte Carlo needed for study of, for instance, metastable states. Moreover, for polymers preserving the integrity of links (i.e. if chain segments cannot pass through each other) mixing of local and non–local moves may result in subtle topological effects leading to a non–uniform sampling of the phase space and eventually to breaking of the balance condition needed for convergence of Monte Carlo scheme to the state of equilibrium¹³. For these and other reasons it is important to examine the conformations of diblock star copolymers in continuous space based on the correct model of hydrophobic–hydrophilic interactions.

The plan of our paper is as follows. First, we briefly summarise the analytical approach used. Then, we present the corresponding results by discussing both the molecular size and the intramolecular conformation. Next, we introduce the model for Monte Carlo simulation and present the results from such an approach performing their comparison with those of the analytical theory. Finally, we discuss the validity and limitations of the Gaussian approach.

II. ANALYTICAL APPROACH

We consider regular star copolymers formed from f equal arms, each consisting of N/f monomers, with a total of $N_{Tot} = N + 1$ monomers, including also the core monomer. On each arm, the monomer beads are sequentially numbered from 1 to N/f starting from the branch point, which is labelled as 0. The beads are connected by freely–jointed bond vectors of unit length oriented outwards. Furthermore, each arm is formed from two blocks of equal lengths, each comprising $N/2f$ beads. One block consists of hydrophobic beads (or, in brief, H-beads, thus forming an H-block), while the other block consists of hydrophilic, or polar, beads (P-beads and P-block). A star polymer with the H-block topologically adjacent to the branch point (and thus with an outer P-block) will be called an INNER-H star, while a star polymer with the opposite connectivity will be called an OUTER-H star. Obviously, the topological location of the H-beads is quite important because in water they would experience a mutually attractive interaction, which eventually determines the chain conformation, and in particular the formation of globular clusters. For simplicity, we shall assume that the type of the bead at the branch point is the same as of the beads in the inner blocks.

The equilibrium conformation of the polymer is then determined by a self–consistent free energy minimisation based on the procedure employed in refs.^{14,15} for linear random copolymers. The intramolecular free energy (see Appendix for more details) consists of the configurational entropy and the intramolecular interactions terms. The latter ones include: (i) the two–body interactions, which can be attractive, repulsive or even vanishing depending on the type of beads involved; (ii) the repulsive screened interactions accounting for the effective “thickness” of the beads; (iii) the repulsive three–body interactions. The last two contributions are assumed to be independent from the type of the interacting beads, unlike the first contribution. Following refs.^{14,15}, we may write it in the Gaussian approximation, as a sum over all pairs of beads of the probability density of contacts multiplied by the interaction constants specifying the sign and strength of these interactions. Thus, the free energy contribution due to the two–body interactions in $k_B T$ units may be written as,

$$\mathcal{A}_2 = \sum_{i < j} B_{ij} \langle r_{ij}^2 \rangle^{-3/2}, \quad (1)$$

where $\langle r_{ij}^2 \rangle$ is the mean-squared distance between beads i, j , and B_{ij} are the interaction constants. The positive and negative signs of these constants mean repulsive and attractive interactions respectively.

Furthermore, following refs.^{15–18} we shall assume in addition that,

$$B_{ij} = \frac{B_i + B_j}{2}, \quad (2)$$

where $B_i > 0$ indicates a P-bead and $B_i < 0$ an H-bead. A rationale for the latter equation was recently presented by two of us (see Eqs. (8-10) in ref.¹⁹). This particular parametrisation of B_{ij} constants results after the effective integration over the solvent molecules degrees of freedom proceeding from the Hamiltonian with a contact monomer-solvent molecules interaction upon the solution incompressibility condition.

For convenience, we may ascribe to each bead a value $y_i = \pm 1$, specifying its P- or H-character, thereby writing B_i in the form,

$$B_i = \sigma y_i + B_0. \quad (3)$$

Thus, σ may be taken as a measure of the copolymer's amphiphilicity, while B_0 characterises the strength of the H-P two-body interactions. In the present paper, we take $B_0 = 0$, so that the latter interactions vanish. It should be remembered, however, that these beads still experience the weaker repulsive interactions (screened and three-body).

Following the general procedure outlined in refs.^{14,20,21} within the framework of Gaussian approximation we can write the intramolecular free energy as a unique function of the average scalar products among the bond vectors, $\langle \mathbf{l}_i \cdot \mathbf{l}_j \rangle$, which are thus the variables subject to optimisation. The only difference of a star polymer with a linear chain is then, clearly, only in the expression yielding the mean-squared distances between beads (on the same or on different arms) in terms of this set of the chosen variational variables. This expression is given and discussed in detail in ref.²² and is not reported here for brevity.

III. RESULTS FROM THE ANALYTICAL APPROACH

Calculations were carried out for 3-arm star copolymers with 16 beads per arm and for 4-arm star copolymers with either 12 or 16 beads per arm. In this way, we could compare stars with either the same number of beads (i.e., $N_{Tot} = 49$ beads) or with the same arm length (i.e., $N/f = 16$ beads). We chose not to impose any symmetry properties upon statistical averages over the arms. This was done to make sure that no asymmetrical conformations were lost (see discussions in ref.¹⁸), although the problem becomes more expensive in terms of computations. A description of the numerical free energy minimisation procedure and the details of all equations expressing various quantities of interest for describing the conformation of a star may also be found in ref.¹⁴.

A. Molecular size

Upon increasing the degree of amphiphilicity σ both INNER-H and OUTER-H stars show clustering of the H-beads into dense globules, but with an essential difference. Formation of a single globule is easily achieved for an INNER-H star through a continuous (second order) transition due to the initial close vicinity of the mutually attractive H-beads thanks to the star connectivity. On the contrary, for an OUTER-H star this is much more difficult to achieve, so that formation of a single globule proceeds through a discontinuous (first order) transition. Furthermore, for these stars a long lived metastable state consisting of f small clusters at the arm ends is also possible.

The smooth collapse transition of an INNER-H star can be followed through the radii of gyration dependence on σ , as shown in Fig. 1 for the 3-arm star (results for the 4-arm stars show a similar pattern and are not shown for brevity). It is useful to consider the mean-squared distance of the H-beads from their own centre of mass, $\langle S_H^2 \rangle$, which decreases monotonously upon increasing σ (i.e. increasing attractive interactions). At the same time, $\langle S_P^2 \rangle$, analogously defined for the P-beads, as well as $\langle S_{Tot}^2 \rangle$, defined as the mean-squared distance of all beads from the common centre of mass, show an initial decrease, which then turns into a steady increase with increasing σ . This behaviour may be easily explained by the increased repulsive potential among the P-beads. It should also be noted that this trend is in addition enhanced by the pull exerted by an increasingly tight core, which brings the arms closer together. As a result, the external P-blocks are highly stretched outwards.

An INNER-H star forms a tight globular core easily if the free energy minimisation uses a random walk conformation as the starting point. In the case of an OUTER-H star the same procedure, however, only leads to a metastable state at large values of σ . Here, the H-beads form f small well separated subglobules at the end of each arm. Coalescence

of these subglobules is prevented by their large spatial separation imposed by the inner P-blocks, which tend to be as far as possible from each other due to their mutual repulsion. Thus, as shown in Fig. 2 with dotted curves for the 3-arm star, in the metastable state $\langle S_P^2 \rangle$ increases monotonously with increasing σ , while $\langle S_{Tot}^2 \rangle$ and $\langle S_H^2 \rangle$ show a shallow dip when the H-blocks do collapse. Further increase of $\langle S_H^2 \rangle$ at larger σ is related to the fact that, while the individual clusters are actually shrinking, they are being pushed afar from the center of mass of the H-beads by the simultaneous stretching of the P-blocks.

The stable equilibrium state of an OUTER-H star can only be found when using a fully collapsed H-star homopolymer with the same total number of beads as the starting point for free energy minimisation. In this stable state, all H-beads cluster together in a single globule. This globule also contains the P-bead of the branch point. The latter feature, however, is not supported by the simulation results in this paper, showing that in the true stable state the core P-bead would actually escape from the hydrophobic core. Apart from this arguable behaviour of the branch point, all other P-beads of the topologically inner blocks form closed swollen loops with an overall daisy-like pattern. These loops tend to be as far as possible from the globular core (as in the stable state of an INNER-H star), but are seriously constrained by the arm connectivity. As a result, in the stable globular state the overall molecular size of an OUTER-H star is quite smaller than the size of the respective INNER-H star.

On the other hand, it is interesting to note that the size of the dense core of H-beads depends only on the total number of beads, but not on the type of star and arms number, i.e. the same $\langle S_H^2 \rangle$ values are obtained for INNER-H and OUTER-H stars with 3 or 4 arms at fixed values of σ and N . This indicates that the molecular topology becomes irrelevant inside dense globules and that their size is dictated only by the space filling requirement, in agreement with previous results²³.

Conversely, for an INNER-H star, using the globular conformation of a fully collapsed H-star homopolymer as the starting point of free energy minimisation results in yet another metastable state. In such a state, the globular core formed by H-beads has essentially the same size as in the stable state, though being less ordered. However, the P-beads tend to be much closer to the common centre of mass, though still protruding outside the globule. This conformation was quite unexpected due to the strong repulsive interactions experienced by the P-beads. As a possible rationalisation for this, we speculate that such a metastable state encompasses a certain number of “knotted” arms with P-blocks being trapped for entropic reasons within the H-core. We do not report such results in Fig. 1 since they are not supported by the computer simulation results.

One should realise that the Gaussian variational theory is, in fact, a mean-field theory which may contain some “unimportant” local minima on the free energy surface. These may either be unstable in some directions or separated by too shallow a barrier from the main minimum, which may thus could be easily overcome due to thermal fluctuations. The latter point is consistent with a relatively poor convergence encountered during the numerical free energy minimisation for this particular metastable state: the final mean-squared gradient of the free energy turned out to be somewhat larger than expected and all further attempts to improve the numerical procedure were plagued by numerical instabilities.

B. Intramolecular conformation

In order to discuss the intramolecular conformation, we shall report some representative results obtained for the 3-arm stars with $\sigma=1.0$. At large values of σ for an INNER-H star the H-beads of the globular core experience a strong attractive interaction, which leads to the formation of a random globule and further to an ordered globule, while the P-blocks stretch outside because of their repulsion. This intramolecular conformation is best described via the mean-squared distances of the beads belonging to a given arm measured from the centre of mass of the polymer. This quantity is shown in Fig. 3a as a function of the position along the arm. We show the plot for only one arm because of the statistical symmetry among the arms found in all cases. The ordering of the hydrophobic core is indicated by the zigzag pattern of the H-beads (black circles in Fig. 3a), which means that the beads lie alternatively on two concentric shells centred at the centre of mass. Correspondingly, the scalar products among the bond vectors connecting the H-beads, $\langle \mathbf{l}_i \cdot \mathbf{l}_{i+k} \rangle$ at fixed i tend to be equal to $(-1)^k$, as was previously reported for short homopolymer chains²⁰. Also, the significantly different distances from the centre of mass for the H- and P-beads give rise to rather different shapes of the density profiles. These density profiles are shown in Fig. 4 using the following dimensionless variables,

$$\hat{\rho}(r) \equiv N_{Tot}^{-1} 4\pi r^2 \langle S_{Tot}^2 \rangle^{1/2} \rho(r), \quad \hat{r} = r / \langle S_{Tot}^2 \rangle^{1/2}, \quad (4)$$

where ρ stands for any of the three functions ρ_H , ρ_P or ρ_{Tot} . Note that each curve is normalized to the fraction of the corresponding beads within the molecule, i.e. N_a/N_{Tot} , index a being H , P , or Tot .

The main features here are the sharp peak for the H-beads related to their tight clustering in the core, and the very broad profile for the P-beads related to their broad distance distribution away from the centre of mass. As a result,

the overall profile of ρ_{Tot} is strongly skewed at large values of r . However, because of the molecular connectivity, no more complicated pattern, such as say a two peak profile, is observed.

In the case of the 3-arm OUTER-H star, the daisy-like pattern of the conformation in the stable state is clearly seen via the mean-squared distances of the beads of a given arm from the centre of mass reported in Fig. 3b (solid line). In particular, the P-beads (white circles) tend to be as far away from the center of mass as possible, thereby maximising their separation, but being constrained by the molecular connectivity they return back to the core of the H-beads. We should note, however, that according to the present results the polar branch point (labelled as $i = 0$) remains trapped within the hydrophobic core. This peculiarity though is not supported by computer simulations results as we have already indicated.

The density profiles for this polymer in Fig. 5 reflect similar features. The density of the H-beads is well localised with a sharp peak at around $\hat{r} = 1/2$ corresponding to a tight packing of these beads in the core. On the contrary, the density of the P-beads is rather delocalised with a shallow peak around $\hat{r} = 1$ corresponding to extended loops of the P-beads. There is also a slightly non-monotonic behaviour observed in $\hat{\rho}_P$ at small \hat{r} related to the trapping of the branch point P-bead within the hydrophobic core. As for the total density, its profile suggests that overall the polymer conformation is only dense around the centre of mass with a fairly long trailing density tail.

Now, if we turn our attention to the conformational structure of the metastable state of the 3-arm OUTER-H star presented in Fig. 3b (dashed curve), we can clearly see an almost linear increase of $\langle R_i^2 \rangle$ with arm index for the P-beads (white circles), reflecting long and rather stretched P-blocks. However, as the arm index reaches 1/2 the mean-squared distances no longer increase, but remain at the same value with small zig-zag oscillations corresponding to ordered small subglobules of the H-beads formed at the ends of the outstretched arms. As in the case of the stable globular core discussed before, the size of these subglobules at a given σ depends only on the number of H-beads they comprise, but not on the number of arms, thus again being dictated by space filling requirement.

Accordingly, the density profiles for this metastable state in Fig. 6 show that the peak in $\hat{\rho}_P$ occurs at smaller \hat{r} than in $\hat{\rho}_H$ and it is marginally higher, so that the H-beads are indeed concentrated at the ends of the P-blocks in the form of f clusters. Finally, the total density has a shape similar to both of the partial densities, though it is about twice higher and has the width of $\hat{\rho}_H$.

IV. CONTINUOUS SPACE MONTE CARLO SIMULATION MODEL

Many previous simulations of star polymers were performed on a lattice. However, any lattice model has a number of serious disadvantages and artefacts. These include rotational anisotropy, tendency for condensed phases to form crystalline structures due to discrete lattice spacing, and dramatic reduction of the acceptance ratio for moves of the core monomer. Thus, we have carried out our simulation in continuous space, which provides by far a more realistic, though somewhat more computationally expensive, description.

The model is implemented for a single star polymer consisting of N_{Tot} monomers connected by harmonic springs between any two monomers i and j within arms of the star, which we denote as $i \sim j$. In addition, all monomers interact with each other via a pair-wise short ranged spherically symmetric potential, so that the Hamiltonian is

$$H = \frac{k_B T}{2\ell^2} \sum_{i \sim j} r_{ij}^2 + \frac{1}{2} \sum_{i \neq j} V_{ij}(r_{ij}). \quad (5)$$

This bead-and-spring model is much more tractable for a Monte Carlo simulation than the freely-jointed model adopted in the analytical part of this work. In any case, since we are interested in rather generic conformational properties of star copolymers, the differences between these implementations of the molecular connectivity should be quite insignificant.

Unlike the Gaussian theory, where for technical reasons one has to introduce a virial-type expansion representing this pair-wise potential, here we can use a more realistic two-body interaction potential explicitly,

$$V_{ij}(r) = \begin{cases} +\infty & \text{for } r < d \\ V_{ij} \left(\left(\frac{d}{r}\right)^{12} - \left(\frac{d}{r}\right)^6 \right) & \text{for } r > d \end{cases}. \quad (6)$$

Thus, monomers are represented by hard spheres of the diameter d , with a short-ranged Lennard-Jones attraction of characteristic strengths V_{ij} . The latter coefficients have the expression akin to Eq. (2),

$$V_{ij} = \frac{V_i + V_j}{2}, \quad (7)$$

where, however, to ensure agreement with Eq. (3) we should take the *Ansatz*,

$$V_i = \sigma(1 - y_i), \quad (8)$$

so that $V_{ij} = 0, \sigma, 2\sigma$ for any P–P, P–H, and H–H pair of monomers respectively. Thus, although the models employed in this section and in the previous one are ideologically the same, they do differ somewhat technically.

During simulation we change the strength of the degree of amphiphilicity σ , which can be viewed as basically the “inverse temperature”, rather than changing the temperature T itself. At $\sigma = 0$ there is only a hard core repulsion, which is represented by a positive three-body coefficient in the virial expansion of the previous section. As a maximal value of the parameter σ we chose $\sigma = 2.5 k_B T$, because in this case the interactions of H–P units are close to those near the theta-point corresponding to vanishing of the second virial coefficient (this is also consistent with the choice of $B_0 = 0$ in Eq. (3)).

The Monte Carlo updates scheme is based on the Metropolis algorithm with local monomer moves employed by two of us in ref.¹¹. The new coordinate of a monomer can be sought as, $q^{new} = q^{old} + r_\Delta$, where q stands for x, y and z spatial projections and r_Δ is a random number uniformly distributed in the interval $[-\Delta, \Delta]$. Here Δ is some additional parameter of the Monte Carlo scheme, which, in a sense, characterises the timescale involved in the Monte Carlo sweep (MCS), the latter being defined as N attempted Monte Carlo steps.

In the current model we work in the system of units such that $\ell = 1, k_B T = 1$, which introduces respective reduced variables for length and energy, and in addition we choose the hard core diameter $d = \ell$.

V. RESULTS FROM MONTE CARLO SIMULATION

Simulations have been carried out for diblock star copolymers with $f = 3, 6, 9, 12$ arms and arm length $N/f = 50$ in all cases. An initial canonical conformation, prepared as a perfect geometrical star in a 2-d plane, is first equilibrated by applying a large number of Monte Carlo sweeps (typically well over $4N_{Tot}^2$ sweeps) at $\sigma = 0$. This procedure allows one to prepare a statistical ensemble (in our case of $Q = 50$) statistically independent homopolymer stars in the swollen coil state. Even though we formally preserve notations of H- and P-beads, in this case all beads experience hard-core repulsions.

This initial statistical ensemble is then used for collapsing each of these stars independently by increasing parameter σ , so that the H-beads become increasingly hydrophobic while the P-beads remain polar, this being done in two possible ways. First, one could perform a quasistatic process, in which σ is changed in 10 small steps until we reach its maximal possible value $\sigma_{max} = 2.5 k_B T$, allowing a long equilibration of the star after each parameter change. In this way we obtain equilibrium conformation for each of these intermediate values of σ . Second, we could perform a sudden change $\sigma = 0 \rightarrow \sigma$ and follow the kinetics of the transition of the initial coil conformation to the final collapsed equilibrium state at σ_{max} . Such kinetic procedure is useful for being able to study formation of possible metastable states, which have been predicted by the analytical theory above.

As for calculation of statistical averages of various observables of interest, for the kinetics one is only allowed to average over values in each of the Q independent members of the statistical ensemble at the same moment in time t , whereas, thanks to the ergodicity property, for the equilibrium states one could average over both the ensemble Q and different moments in time (i.e. different Monte Carlo sweeps well separated from each other to improve statistical independence). The latter allows one to obtain much better statistics and hence smoother curves in case of equilibrium measurements, while getting the same quality for the kinetics would seem too time consuming.

Now, we are going to compare the results from the computer simulation with those of the analytical Sec. III. A typical snapshot of the equilibrium collapsed state of the INNER-H star is shown in Fig. 7. Indeed, there is a nearly spherical dense core of fully collapsed H-beads (black colour) and rather outstretched P-blocks (gray colour) hands sticking out of it in a micellar fashion. Now, if we compare the corresponding plots in Figs. 8 and 3a for $\langle R_i^2 \rangle$ vs the arm index, bearing in mind the difference between the theoretical and simulation models and different sizes of considered stars, the agreement between them seems very striking indeed. We may also observe from Fig. 8 that the larger is the star (i.e. greater f), the larger is its size and the higher is the slope of an increasingly linear increase of $\langle R_i^2 \rangle$ with the arm index for the P-beads. A zig-zag pattern for the H-beads is absent in Fig. 8 because the bead-and-spring model does not lead to any particular ordering of the globule, contrary to the freely-jointed chain model, in which bonds have to be arranged in a special manner consistent with close packing. Yet, the observed behaviour indicates a rather universal character of the subject in hand.

Let us now compare partial and total densities in Figs. 9 and 4. Despite the obvious limitations of the Gaussian approximation, in which densities can only be represented by a sum of Gaussoids, we still do find a good general agreement between theory and simulations once we are comparing reduced dimensionless densities $\hat{\rho}$ vs \hat{r} . The overall shapes, as well location of peaks and their heights, for all three curves appear to be rather consistent. To avoid any

repetition of their discussion already presented in Sec. III, we would like to concentrate instead on the distinctions, thereby clearly establishing possible limitations of the theory. First of all, a sum of Gaussoids can never produce a rather flat shape. Thus, the density of the P-beads, $\hat{\rho}_P$, is practically zero in Fig. 9 until almost $\hat{r} \simeq 0.4$ (i.e. within the H-core), while it cannot possibly be so in Fig. 4 being a sum of Gaussoids. Apart from that feature, for the H-beads $\hat{\rho}_H$ does vanish abruptly, while $\hat{\rho}_P$ and $\hat{\rho}_{Tot}$ do have long tails, for $\hat{r} > 1$ in both Figs. 9 and 4. To satisfy the normalisation conditions, because of a somewhat different behaviour of $\hat{\rho}_P$ near the centre of mass, all densities in the Gaussian theory have to be somewhat deformed as compared to their precise shape in the computer simulation. Nevertheless, the density plots seem quite consistent with each other, and particularly so for the total density.

Now then, we turn our attention to the OUTER-H stars. In Fig. 10 we exhibit a snapshot of the 12-arm star in the stable equilibrium state obtained by a quasistatic change of σ with attendant long equilibration after every step. The structure does indeed have a nearly spherical collapsed H-core (black beads), with the P-blocks (gray beads) looping out in a daisy-like manner. Clearly, the branch point P-bead (black clubsuit) has been able to escape outside the core in all of the many analysed members of the ensemble, and it is the centre to which all other P-blocks are attached by harmonic springs. Overall structure is much more compact than in Fig. 7 and this is also reflected in the graphs in Fig. 11 compared to those of Fig. 3b. In order to avoid over-emphasising the good general agreement again, let us instead remark that the branch P-bead is trapped around the centre of mass in the analytical result of Fig. 3b, producing too small values of $\langle R_i^2 \rangle$ for neighbouring to it P-beads as opposed to the simulation results in Fig. 10. In the latter, all P-beads are clearly farther away from the centre of mass than any of the H-beads, and this behaviour seems to make more sense physically. Thanks to the availability of data for different values of f , one can also see increasingly better ability of looping of the P-blocks in stars with larger number of arms, so that the $\langle R_i^2 \rangle$ plot becomes more and more symmetrically bell-shaped on the left.

Density profiles in Figs. 12 and 5 again have consistent overall shapes, peak locations and heights, except that $\hat{\rho}_P$ is vanishing for $\hat{r} < 0.5$ in the simulation results and it cannot possibly be so in the Gaussian theory for the reason already outlined.

Now, let us examine the state obtained as a result of the kinetic process of star collapse after a sudden quench of $\sigma = 0 \rightarrow \sigma_{max}$. The corresponding snapshot is presented in Fig. 13 and it does look like a star consisting of f P-arms with small H-subglobules at their ends, as predicted by the analytical theory. This state was found to be a rather long-lived metastable one for quenches to $\sigma_{max} \leq 2.5$ — the associated nucleation time needed to overcome the barrier for transformation to the equilibrium state of Fig. 10 was clearly much longer than the Monte Carlo times practically accessible to our computational resources (which consisted of a 16-node Beowulf PII-400 MHz cluster). However, we have also found that for much deeper quenches the nucleation regime would transform into the spinodal decomposition one, in which the state of Fig. 13 becomes unstable, so that the kinetics quickly passes through this intermediary to achieve the final equilibrium structure.

Looking at the observables such as the mean squared distances and densities as measured from the centre of mass, there is a good agreement of Figs. 14 and 3b, as well as Figs. 15 and 6, even though in the one case a kinetic procedure was used, while a local free energy minimum was used in the other. We note also that the statistical quality of Figs. 14 and 15 is poorer than of similar equilibrium plots presented before for obvious reasons, yet it is quite satisfactory to resolve the shapes well. The kinetically obtained densities are somewhat broader, which possibly reflects a better ability of P- and H- beads to move and mix within their preferred regions of space.

These observations allow us to firmly conclude that the current metastable state of OUTER-H stars is indeed a robust metastable state under the considered values of the degree of amphiphilicity σ , while it becomes an unstable kinetic intermediary for deeper quenches, consistent with the general theory of phase transitions and many of concrete examples of similar behaviour previously seen by us for conformational transitions of other polymeric systems^{11,18}.

Finally, it would be interesting to study the effect of changing the composition ratio of H:P monomers within the arms at a given arms number, for instance $f = 6$. Thus, we have studied the following ratios $N_H/N_{Tot} = 0.2, 0.4, 0.6, 0.8$ as well as the homopolymers $N_H/N_{Tot} = 0, 1$ in addition to the cases of symmetric diblocks $N_H/N_{Tot} = 0.5$ studied for both INNER-H and OUTER-H topologies. First of all, we find that the above general conclusions about the existence of a metastable state for OUTER-H stars as well as the structures of conformations remain valid in a rather broad range of composition ratios.

In Fig. 16 we present the dependence of the mean-squared radius of gyration on the H:P ratio for the three respective structures in poor solvent. Obviously, the size of all three structures decreases monotonically with increasing number of the H-beads. Our conclusion that the OUTER-H globules are more compact than the INNER-H ones remains true here throughout, being most pronounced around small values of N_H/N_{Tot} , in this case near 0.2. Interestingly, the large-size metastable state for OUTER-H stars exists for all concentrations except very near the two limiting homopolymer cases. Moreover, no other metastable states have been seen in kinetics.

In Figs. 17,18,19 we exhibit the mean-squared distances of monomers from the centre of mass for the INNER-H, OUTER-H and metastable OUTER-H states respectively. Naturally, the shapes of these curves experience predictable and monotonic shifts, reflecting the changes of the lengths of the H- and P-blocks. So, $\langle R_i^2 \rangle$ for the INNER-H structure

remains nearly constant within the collapsed H-core, starting to grow characteristically for the P-corona beads with increasing chain index i . This function for the stable state of OUTER-H stars has a familiar bell-shape for the P-units, forming loops around the collapsed H-core, for which the function remains nearly constant. And for the metastable state of the OUTER-H stars we have a steady growth of $\langle R_i^2 \rangle$ as long as i belongs to the P-block, which changes to a nearly constant behaviour when i reaches the H-block. Such types of behaviour are fully consistent with the structures seen in snapshots for the symmetric diblocks. It is also interesting to follow in more detail the separation of the core monomer $i = 0$ from the centre of mass. For the INNER-H globules the core monomer remains very close to the centre of mass similarly to the simple homopolymer star. The same conclusion is also true for the metastable OUTER-H structures, whereas for the stable OUTER-H state $\langle R_0^2 \rangle$ is quite large, especially for small N_H/N_{Tot} ratios due to long loops formed by the P-beads to all of which the core monomer is connected.

VI. CONCLUSION

In the present paper we have studied the behaviour of block copolymer stars in dilute solution by means of analytical Gaussian variational theory and Monte Carlo simulation in continuous space. We considered stars with each arm consisting of a diblock chain, one block being formed by hydrophilic (polar) monomers or P-beads, and the other one by hydrophobic monomers or H-beads. Moreover, we were interested in symmetric stars either having the H-block connected to the core bead and with the P-block being outside — an INNER-H star, or having the opposite connectivity — an OUTER-H star. In both cases, we have found that for a sufficiently large degree of amphiphilicity the stable state corresponds to conformations with a dense globule formed by the H-beads, which is surrounded by the P-blocks stretching outwards. However, because of the intramolecular connectivity, the OUTER-H stars have a considerably smaller overall size than the INNER-H ones. Indeed, the P-beads have to return back towards the globule of the H-beads and they are all connected to the same core monomer.

Interestingly, for a given degree of amphiphilicity, the size of the H-globule turns out to depend only on the number of H-beads, but it is basically independent of the star topology (i.e. whether it is an INNER-H or an OUTER-H star), and only rather weakly dependent on the number of arms. The latter dependence is related to the repulsive interactions among the P-beads, whose number increases with the star functionality.

Another interesting result of our study was in finding that there is a metastable state for the OUTER-H stars. The conformation corresponding to this state looks precisely as a swollen mini-star with the H-beads clustering into small subglobules at the ends of the outstretched P-blocks. The repulsive interactions of the inner P-beads and an entropic barrier prevent the coalescence of these small subglobules into a single globule, as it is the case in the stable state. Importantly, this metastable state was also found by the Dynamic Monte Carlo simulation during kinetics after a sudden quench from the swollen coil to the poor solvent regime. This kinetic intermediary appears to be a rather long-lived metastable state separated by a nucleation stage from the final equilibrium state. We have also seen that this nucleation regime would transform into a spinodal regime rendering such a state unstable during kinetics after a much deeper quench (i.e. larger degree of amphiphilicity).

One may argue that the existence of such a metastable state would have an obvious implication for the phase diagram of these stars. Indeed, the attractive interactions among the H-beads, which lead to the intramolecular formation of the small droplets at the ends of the arms, would also lead to star aggregation through intermolecular interactions and, eventually, to phase separation. Conversely, in the stable state, the inner globules of two molecules would not aggregate as easily because they are shielded by the outer P-beads exhibiting mutually repulsive interactions, which therefore act as colloidal stabilisers.

We have also studied diblock stars with varying H:P composition ratio and have found that the above general conclusions, such as e.g. the existence of the OUTER-H metastable state, remain valid for a very broad range of composition ratios. The family of plots for the mean-squared distances of monomers from the centre of mass versus the chain index has been systematically obtained, but it uncovers only very predictable patterns.

Given a certain technical distinction in the models adopted by the analytical Gaussian theory and the Monte Carlo simulation, as well as expected limitations of the former due to approximations involved, we have found a very good agreement in the results from both techniques. This is a clear indication that the behaviour we are seeing is indeed universal, and it is not really affected by the analytical approximations or implementation of the simulation.

Speaking of small discrepancies between the results, one should mention the trapping of the core P-bead within the H-globule in the stable state of OUTER-H stars as seen by the analytical theory. However, all simulation results indicate that this bead can actually escape from the globule, clearly leading to a more energetically favourable situation. The trapping is possibly enhanced by the small number of degrees of freedom for short lengths of the arms, but in any case is believed to be an artefact of the theory.

Perhaps one of the most impressive agreements in the results was obtained for the density profiles, as long as one

used the reduced variables $\hat{\rho}_a$ vs \hat{r} , with a being P , H , or Tot . Even though the numbers of arms and their lengths differed significantly in both considered cases, the plots in terms of the reduced dimensionless variables showed a robust consistency with each other. This may seem unexpected given that the density can only be expressed via a superposition of Gaussian-shaped functions within the analytical theory. One noticeable discrepancy with the simulation results was found, however, for $\hat{\rho}_P$ in the stable globular state of the INNER-H and OUTER-H stars within the range $\hat{r} \leq 1$. In that region, the density of the P-beads goes quickly to zero for $\hat{r} \leq 0.5$ in the results of the simulation, showing a perfect P-beads expulsion from the space occupied by the dense H-subglobule. This behaviour, however, manifests itself only in a relatively moderate density decrease in case of the Gaussian theory, which on the other hand somewhat distorts the overall density shape due to the normalisation requirement. Apart from this understandable difference, the overall shapes, peaks locations, heights and widths are in good agreement between the theory and simulation.

The overall good agreement of the Gaussian variational theory with the simulation in application to such complicated a system as a diblock copolymer star, demonstrates the strength of the theory for predicting the details of polymer conformations. The main idea of the Gaussian variational theory is in determining the effective connectivity matrix between all beads which would mimic the true intramolecular interactions in the most optimal way, i.e. minimise the trial free energy, $\mathcal{A}_{trial} = \mathcal{A}_0 + \langle H - H_0 \rangle_0$, where H_0 and \mathcal{A}_0 are the trial Hamiltonian and free energy associated with it. The choice of variational variables differs somewhat in the two versions of the theory: it involves products of bond vectors $\langle \mathbf{l}_i \cdot \mathbf{l}_j \rangle$ in the Milan version, while the set of mean squared distances $\langle (\mathbf{X}_i - \mathbf{X}_j)^2 \rangle$ between monomers in the Dublin version. However, as it is demonstrated in the Appendix below, the resulting free energy expressions are in fact the same, up to a trivial additive constant and some rescaling of the parameters of the model. In so far as the phase diagram and behaviour of simple observables, such as e.g. radius of gyration, mean-squared distances and density profiles, are concerned, the Gaussian self-consistent approximation turns out to be quite accurate. It is also clear that the variational theory should become increasingly successful in dealing with polymers with complex intramolecular architecture as compared to linear chain polymers precisely because the conformation of the former polymers is more dictated by the connectivity constraints.

Furthermore, the current theory also permits extensions to the realm of kinetics by writing time-dependent equations for instantaneous values of the adopted averaged variables in terms of the instantaneous free energy gradients (see. e.g. ref.¹⁸). Such future kinetic studies of copolymers with complex topology present a considerable interest. To illustrate this point, we may mention that folding of even a homopolymer star proceeds considerably faster than of the equivalent linear chain, and this is even more so for an INNER-H star vs diblock linear chain. In certain cases of “random” copolymers with a specially optimised complex topology one may achieve a much more efficient and faster folding than for the equivalent linear chain, which would yet produce a globule with an almost identical conformational structure since the connectivity constraints are less relevant within the dense globule. This may present certain new insights and opportunities for the broad areas of biopolymer folding and perhaps even drug delivery.

Speaking of more traditional applications, we believe that the results of this work may facilitate some further experimental research on copolymer stars with a view of their applications such as as viscosity modifiers and coating additives. On the one hand, the existence of distinct stable compact and semi-extended conformational states with good colloidal stabilisation properties seems of certain interest. The presence of the semi-extended metastable state with “sticky” properties, moreover, indicates that copolymer stars in solutions at higher concentrations may exhibit a spectacular phase behaviour. While this is interesting, the studies of aggregation phenomena within the present very detailed treatment are not particularly justified due to considerable computational expenses. A somewhat more coarse-grained approach, both analytically and in terms of the Monte Carlo model, may lead to a faster progress in this direction. We expect that appropriate techniques for such analysis could soon be developed and that the corresponding complex phenomena will be thoroughly studied within the next few years. Finally, we would like to express a hope that the theoretical and computational study of macromolecular solutions involving polymers with increasingly complex design, as well as the collaboration between our two Groups, will continue in the future.

ACKNOWLEDGMENTS

The authors are thankful to Professor Giuseppe Allegra, Professor Angelo Perico and Dr Guido Raos for interesting discussions. One of us (E.T.) would like to thank Gavin McCullagh and Ronan Connolly for their work on the related GUI environment and gaining preliminary insights into the problem during the course of their undergraduate projects.

This work was supported by grant IC/1999/01 from Enterprise Ireland, which has helped to develop a fruitful collaboration between the Dublin and Milan Groups.

APPENDIX: MATHEMATICAL DETAILS AND NOTES ON THE GAUSSIAN METHOD

Comparison of the results from the theory and simulation using different models of connectivity in this paper show that as far as the universal properties of polymers are concerned one could use either of the two models: freely-jointed or bead-and-spring one. Since the connectivity term (5) is the only one which is affected by the molecular topology, it would suffice to discuss the theory for a linear polymer chain, in which one has to change the connectivity matrix appropriately.

The purpose of this Appendix is to give some mathematical details on the analytical equations employed, but as an added bonus to demonstrate the equivalence of the equilibrium free energy expressions used independently by the two Groups. Thus, let us establish an explicit relationship between the free energy of the GSC method in ref.¹⁸ and that of refs.^{14,21}.

First of all, monomer coordinates can be written for a linear chain via the bond vectors as follows, $\mathbf{X}_i = \sum_{j=0}^i \mathbf{l}_j$, if we choose the reference point as, $\mathbf{X}_0 = 0$. Then, the mean squared distances between monomers i and j are written as

$$D_{ij} \equiv \frac{1}{3} \langle (\mathbf{X}_i - \mathbf{X}_j)^2 \rangle. \quad (\text{A1})$$

Therefore, the entropic term (Eq. (7) in ref.²¹) in units of $k_B T = 1$,

$$\mathcal{A}_{el} = \frac{3}{2} (\text{Tr } \mathbf{M} - \ln \text{Det } \mathbf{M}), \quad (\text{A2})$$

where we have discarded a constant independent of the variational variables and the matrix \mathbf{M} defined as,

$$M_{ij} \equiv \frac{1}{l^2} \langle \mathbf{l}_i \cdot \mathbf{l}_j \rangle \quad (\text{A3})$$

can be rewritten as follows. Its first part becomes the harmonic springs “energy” (Eq. (10) in ref.¹⁸),

$$\mathcal{E}_{sp} = \frac{3}{2\ell^2} \sum_{i \sim j} D_{ij}, \quad \ell \equiv \frac{l}{\sqrt{3}}, \quad (\text{A4})$$

which in the latter form would also be valid for stars and any other topology as it is precisely the first term in Eq. (5) employed in Sec. IV.

Now, let us consider the determinant of the matrix \mathbf{M} , where we have scaled out the constant l ,

$$\begin{pmatrix} \langle \mathbf{l}_1 \cdot \mathbf{l}_1 \rangle & \langle \mathbf{l}_1 \cdot \mathbf{l}_2 \rangle & \dots & \langle \mathbf{l}_1 \cdot \mathbf{l}_{N-1} \rangle \\ \langle \mathbf{l}_2 \cdot \mathbf{l}_1 \rangle & \langle \mathbf{l}_2 \cdot \mathbf{l}_2 \rangle & \dots & \langle \mathbf{l}_2 \cdot \mathbf{l}_{N-1} \rangle \\ \dots & \dots & \dots & \dots \\ \langle \mathbf{l}_{N-1} \cdot \mathbf{l}_1 \rangle & \langle \mathbf{l}_{N-1} \cdot \mathbf{l}_2 \rangle & \dots & \langle \mathbf{l}_{N-1} \cdot \mathbf{l}_{N-1} \rangle \end{pmatrix}. \quad (\text{A5})$$

Obviously, the determinant of a matrix does not change if one adds a column or a row to any other columns or rows. Thus, by adding the first row to the second, then the new second to third and so on, we obtain,

$$\begin{pmatrix} \langle \mathbf{X}_1 \cdot \mathbf{l}_1 \rangle & \langle \mathbf{X}_1 \cdot \mathbf{l}_2 \rangle & \dots & \langle \mathbf{X}_1 \cdot \mathbf{l}_{N-1} \rangle \\ \langle \mathbf{X}_2 \cdot \mathbf{l}_1 \rangle & \langle \mathbf{X}_2 \cdot \mathbf{l}_2 \rangle & \dots & \langle \mathbf{X}_2 \cdot \mathbf{l}_{N-1} \rangle \\ \dots & \dots & \dots & \dots \\ \langle \mathbf{X}_{N-1} \cdot \mathbf{l}_1 \rangle & \langle \mathbf{X}_{N-1} \cdot \mathbf{l}_2 \rangle & \dots & \langle \mathbf{X}_{N-1} \cdot \mathbf{l}_{N-1} \rangle \end{pmatrix}. \quad (\text{A6})$$

By repeating the same procedure for the columns, likewise we conclude that

$$\text{Det } \mathbf{M} = \text{Det } \mathcal{F}, \quad \mathcal{F}_{ij} \equiv \frac{1}{l^2} \langle \mathbf{X}_i \cdot \mathbf{X}_j \rangle, \quad (\text{A7})$$

which in turn agrees with Eqs. (B3) and (B5) in ref.¹⁸ upon fixing the reference point at $\mathbf{X}_0 = 0$.

Finally, the virial expansion of the excluded volume energy (Eq. (10) in ref.¹⁸),

$$\mathcal{E}_{exc} = \sum_{J=2}^{\infty} \sum_{\{i\}} B_{\{i\}}^{(J)} (\text{Det } \Delta^{(J-1)})^{-3/2}, \quad \Delta_{rs}^{(J-1)} \equiv \frac{1}{3} \langle (\mathbf{X}_{i_1} - \mathbf{X}_{i_{r+1}}) \cdot (\mathbf{X}_{i_1} - \mathbf{X}_{i_{s+1}}) \rangle, \quad (\text{A8})$$

expands into the following explicit formulae for the determinants appearing in the two- and three-body interaction terms,

$$\text{Det}\Delta_{ii'}^{(1)} = D_{ii'} \quad (\text{A9})$$

$$\begin{aligned} \text{Det}\Delta_{ii' i''}^{(2)} &= \begin{vmatrix} D_{ii'} & \frac{1}{2}(D_{ii'} + D_{ii''} - D_{i'i''}) \\ \frac{1}{2}(D_{ii'} + D_{ii''} - D_{i'i''}) & D_{i'i''} \end{vmatrix} = \\ &= \frac{1}{2}(D_{ii'} D_{ii''} + D_{ii'} D_{i'i''} + D_{ii''} D_{i'i''}) - \\ &\quad - \frac{1}{4}(D_{ii'}^2 + D_{ii''}^2 + D_{i'i''}^2). \end{aligned} \quad (\text{A10})$$

These are precisely the expressions for the two-body and three-body interaction energy terms as in Eqs. (50,51) of ref.²¹. The positiveness of the first determinant requires all mean squared distances to be positive, $D_{ii'} > 0$, which is true as this is the average of a quantity squared. The positiveness of the three-body determinant in Eq. (A10), on the other hand, is insured by the triangle inequality,

$$D_{ii''}^{1/2} < D_{ii'}^{1/2} + D_{i'i''}^{1/2}. \quad (\text{A11})$$

It is interesting to note that the quantity $(\text{Det}\Delta_{i_1, \dots, i_J}^{(J-1)})^{3/2}$ characterises the volume of the phase space occupied by J particles if the mean squared distances between all pairs are specified. Moreover, the logarithm of this characteristic volume of all N particles is equal to the variational entropy of the system up to a trivial constant,

$$\text{Det}M = \frac{1}{N^2} \text{Det}\Delta^{(N-1)}. \quad (\text{A12})$$

This completes establishing the equivalence of the variational free energy expressions between the methods — one which is based on bond-vectors^{14,15,20,21} and another which is based on the monomer coordinates and mean squared distances between monomers^{11,16-19}.

¹ V. Degiorgio, M. Corti, Eds., “*Physics of Amphiphiles: Micelles, Vesicles, and Microemulsions*”, North-Holland, Amsterdam **1985**.

² J. Israelachvili, “*Intermolecular and Surface Forces*”, Academic, London **1991**.

³ K. A. Dill, S. Bromberg, K. Yue, K. M. Fiebig, D. P. Yee, P. D. Thomas, H. S. Chan, *Protein Sci.* **1995**, *4*, 561.

⁴ D. E. Leckband, O. V. Borisov, A. Halperin, *Macromolecules* **1998**, *31*, 2368.

⁵ A. Yu. Grosberg, A. R. Khokhlov, “*Statistical Physics of Macromolecules*”, AIP Press, New York **1994**.

⁶ Y. Rouault, *Macromol. Theory Simul.* **1998**, *7*, 359.

⁷ N. Hadjichristidis, S. Pispas, M. Pitsikalis, H. Iatrou, C. Vlahos, *Adv. Polym. Sci.* **1999**, *142*, 71.

⁸ G.S. Grest, L. J. Fetters, J. S. Huang, *Adv. Chem. Phys.* **1996**, *94*, 67.

⁹ J. J. Freire, *Adv. Polym. Sci.* **1999**, *143*, 35.

¹⁰ P. H. Nelson, G. C. Rutledge, T. A. Hatton, *Comp. Theor. Polym. Sci.* **1998**, *8*, 31.

¹¹ Yu. A. Kuznetsov, E. G. Timoshenko, *J. Chem. Phys.* **1999**, *111*, 3744.

¹² L. A. Molina, J. J. Freire, *Macromolecules* **1999**, *32*, 499.

¹³ Yu.A. Kuznetsov, E.G. Timoshenko, *Progr. Colloid Polym. Sci.* **2000**, *115*, 146.

¹⁴ F. Ganazzoli, *J. Chem. Phys.* **1998**, *108*, 9924.

¹⁵ F. Ganazzoli, *J. Chem. Phys.* **2000**, *112*, 1547.

¹⁶ E. G. Timoshenko, Yu. A. Kuznetsov, K. A. Dawson, *Phys. Rev. E* **1996**, *53*, 3886.

¹⁷ E. G. Timoshenko, Yu. A. Kuznetsov, K. A. Dawson, *Phys. Rev. E*, **1997**, *55*, 5750.

¹⁸ E. G. Timoshenko, Yu. A. Kuznetsov, K. A. Dawson, *Phys. Rev. E* **1998**, *57*, 6801.

¹⁹ E. G. Timoshenko, Yu. A. Kuznetsov, *J. Chem. Phys.* **2000**, *112*, 8163.

²⁰ F. Ganazzoli, *Macromol. Theory Simul.* **1997**, *6*, 351.

²¹ G. Raos, G. Allegra, F. Ganazzoli, *J. Chem. Phys.* **1994**, *100*, 7804.

²² G. Allegra, E. Colombo, F. Ganazzoli, *Macromolecules* **1993**, *26*, 330.

²³ G. Allegra, M. De Vitis, F. Ganazzoli, *Macromol. Chem., Theory Simul.* **1993**, *2*, 829.

FIG. 1. The mean-squared radii of gyration of the 3-arm INNER-H star copolymer (in units of the bond length l) as a function of the amphiphilicity parameter σ . The H, P and Tot labels indicate the mean-squared radius of gyration of the H-beads, of the P-beads and of the whole molecule, respectively.

FIG. 2. The same plots as in Fig. 1, but for the 3-arm OUTER-H star copolymer. The dotted lines correspond to the metastable states, and the vertical dash-and-dot line at $\sigma \simeq 0.25$ is the tie line connecting the stable states with the same free energy.

FIG. 3. The mean-squared distances of the beads from the common centre of mass, $\langle R_i^2 \rangle$, (in units of the bond length l) of the 3-arm INNER-H star at $\sigma = 1.0$ (part a, on the left) and OUTER-H star (part b, on the right). The lower solid curve corresponds to the stable state and the upper dashed curve to the metastable state, plotted as a function of the bead position along an arm. Here $i = 0$ is the branch point, $i = N/f$ is the free end. Only the beads of one arm are shown due to the molecular symmetry obtained in all states. The black circles indicate the H-beads and the white circles the P-beads. The vertical dotted line at $\frac{i}{N/f} = 0.5$ indicates the last bead of the inner block.

FIG. 4. The dimensionless reduced density $\hat{\rho}(r)$ profiles vs the dimensionless distance \hat{r} (see Eq. (4)) for the same INNER-H star as in Fig. 3a. These densities are drawn for the H-beads, P-beads and all beads. The normalisation condition for each of these functions are simply, $\int_0^\infty d\hat{r} \hat{\rho}_a(r) = \frac{N_a}{N_{Tot}}$.

FIG. 5. The dimensionless density profiles vs the dimensionless distance for the 3-arm OUTER-H star in the stable state at $\sigma = 1.0$ drawn as in Fig. 4.

FIG. 6. The dimensionless density profiles vs the dimensionless distance for the 3-arm OUTER-H star in the metastable state at $\sigma = 1.0$ drawn as in Fig. 4.

FIG. 7. A snapshot of the conformation of the INNER-H 12-arm star. Here and in all other figures from the Monte Carlo simulation $\sigma = 2.5$ and the colours are assigned as follows: black to H-beads, grey to P-beads, and clubsuit to the central monomer. We should also emphasise that the balls size is not up to scale in these snapshots and has been adjusted simply to look well on paper.

FIG. 8. The mean-squared distances of the beads from the centre of mass, $\langle R_i^2 \rangle$, (in units of the bond length l) vs their position along an arm, $i/(N/f)$, for the INNER-H stars with $f = 3, 6, 9, 12$ (from bottom to top) obtained from Monte Carlo simulation. Here and below, each star's arm consists of 50 monomers, and the amphiphilicity parameter is $\sigma = 2.5$.

FIG. 9. The dimensionless density profiles $\hat{\rho}$ vs the dimensionless distance \hat{r} for the INNER-H star with $f = 12$ arms obtained from Monte Carlo simulation. Here the thin solid curve, the dashed curve and the thick solid curve correspond to densities of the H-beads, P-beads and all beads respectively.

FIG. 10. A snapshot of the conformation of the OUTER-H 12-arm star in the stable state at $\sigma = 2.5$. The central monomer is clearly visible here on the outside.

FIG. 11. The plots of $\langle R_i^2 \rangle$ vs $i/(N/f)$ drawn as in Fig. 8, but for OUTER-H stars in the stable state, obtained from Monte Carlo simulation.

FIG. 12. The profiles of $\hat{\rho}$ vs \hat{r} as in Fig. 9, but for OUTER-H star in the stable state, obtained from Monte Carlo simulation. The same curve notations apply here also.

FIG. 13. A snapshot of the conformation of the OUTER-H 12-arm star in the metastable state at $\sigma = 2.5$. Note that not all of $f = 12$ arms may be well distinguishable here in a 2-d projection of the 3-d conformation of the polymer.

FIG. 14. The plots of $\langle R_i^2 \rangle$ vs $i/(N/f)$ drawn as in Fig. 8, but for OUTER-H stars in the metastable state, obtained from Monte Carlo simulation.

FIG. 15. The profiles of $\hat{\rho}$ vs \hat{r} as in Fig. 9, but for OUTER-H star in the metastable state, obtained from Monte Carlo simulation. The same curve notations also apply.

FIG. 16. Plot of the mean squared radius of gyration, $\langle S^2 \rangle$, vs the composition ratio of hydrophobic units, N_H/N obtained from Monte Carlo simulation. Here and below, each star consists of $f = 6$ arms. Note that the leftmost and rightmost points correspond to homopolymer stars consisting of hydrophilic and hydrophobic monomers respectively. The curve denoted by OUTER-H_m corresponds to the metastable state.

FIG. 17. The mean-squared distances of the beads from the centre of mass, $\langle R_i^2 \rangle$, (in units of the bond length ℓ) vs their position along an arm, $i/(N/f)$, for INNER-H stars. Solid lines correspond to homopolymer stars consisting of hydrophilic (upper curve) and hydrophobic (lower curve) monomers. Here and below other lines correspond to stars with the composition ratios $N_H/N = 0.2, 0.4, 0.6$ and 0.8 (from top to bottom).

FIG. 18. The plots of $\langle R_i^2 \rangle$ vs $i/(N/f)$ drawn as in Fig. 17, but for OUTER-H stars in the stable state.

FIG. 19. The plots of $\langle R_i^2 \rangle$ vs $i/(N/f)$ drawn as in Fig. 17, but for OUTER-H stars in the metastable state.

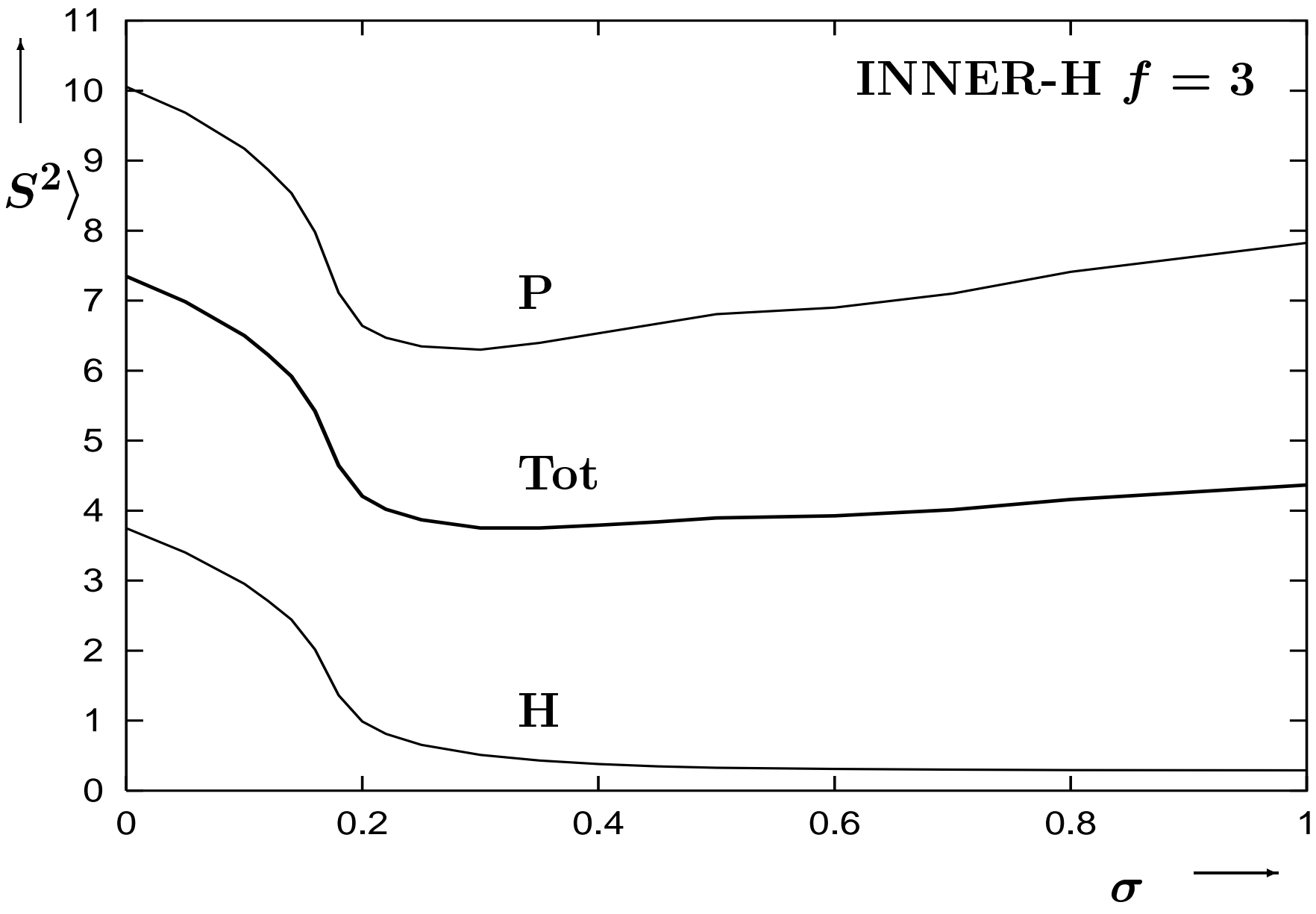


Fig. 1

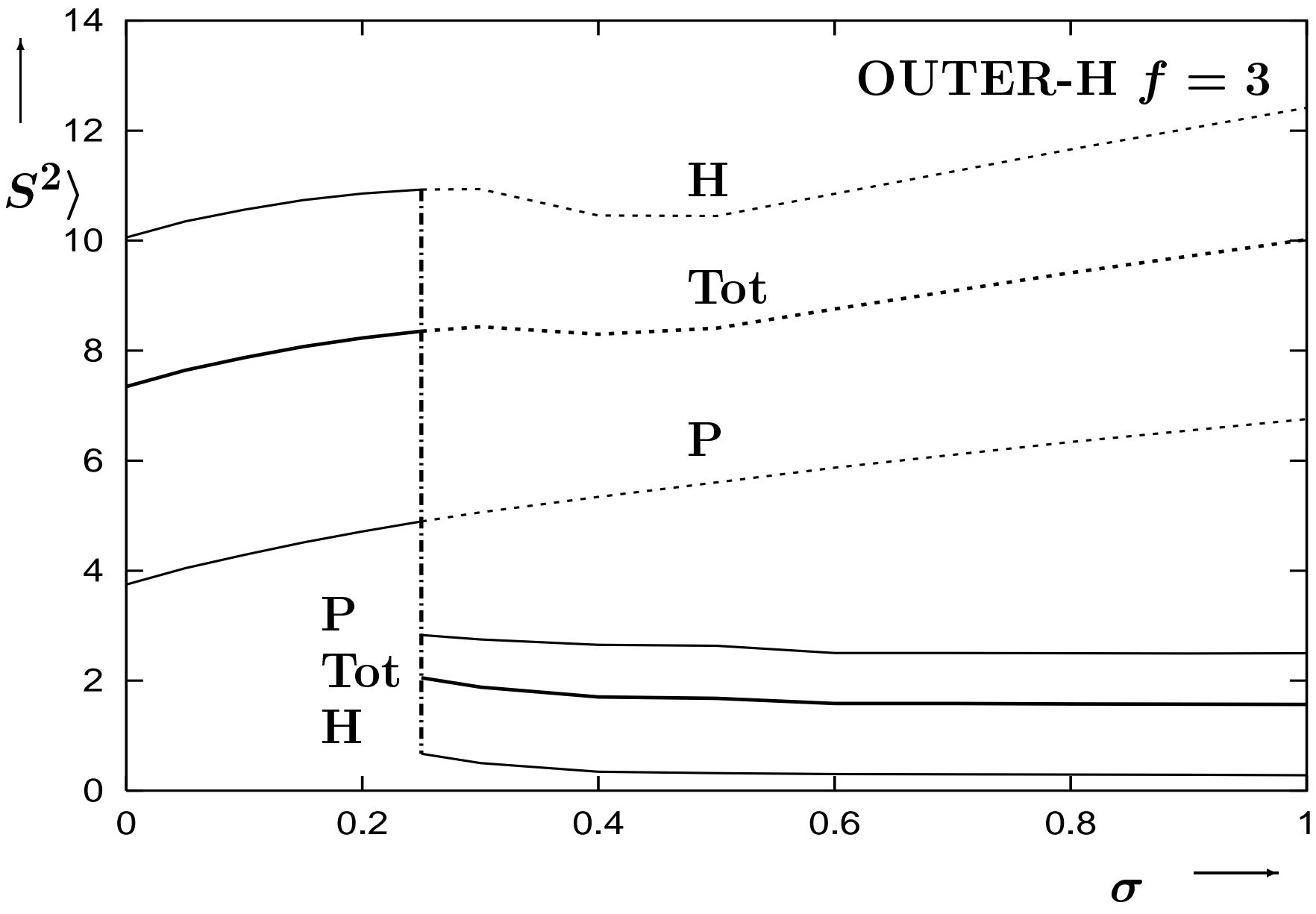


Fig. 2

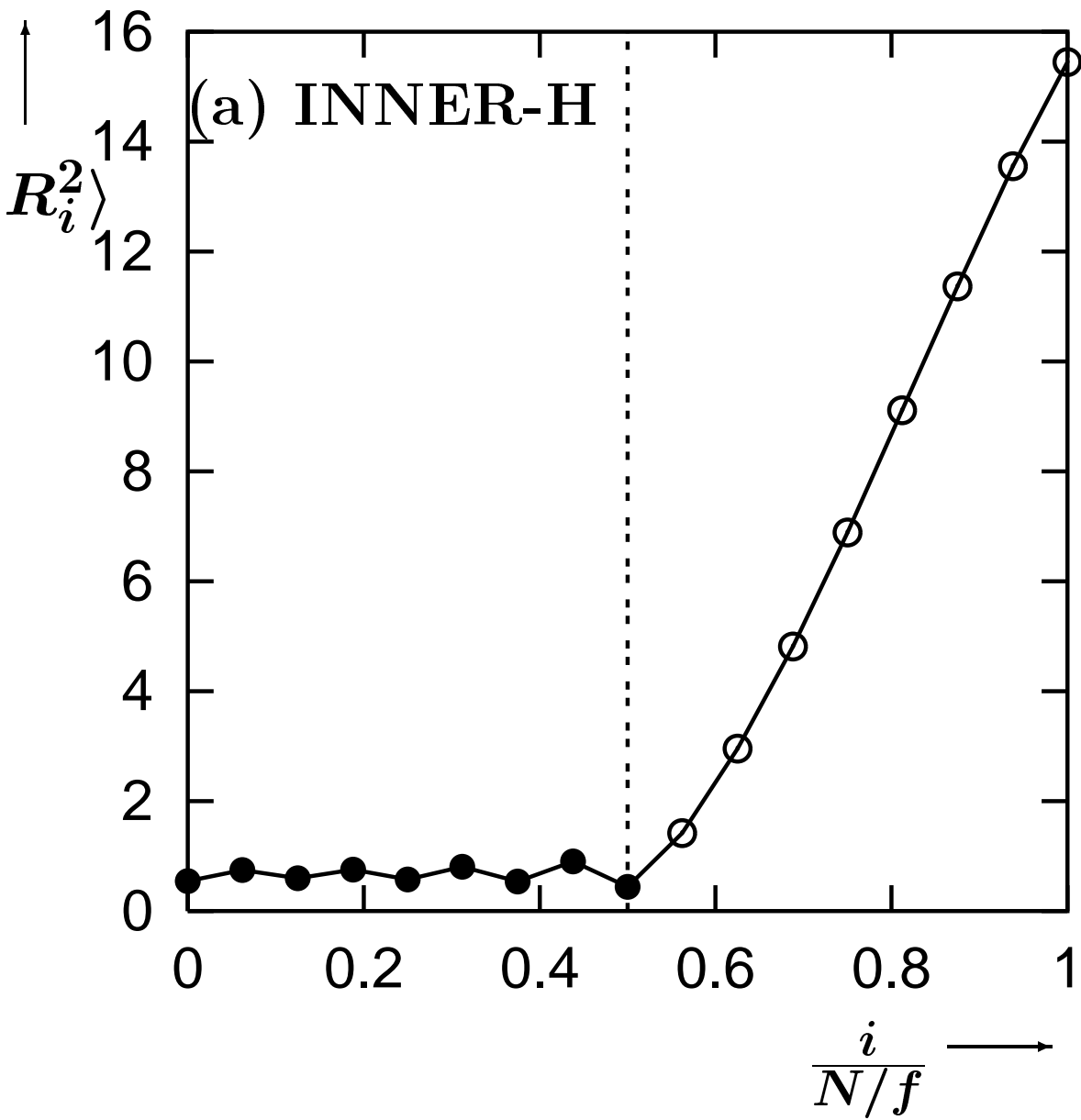


Fig. 3a

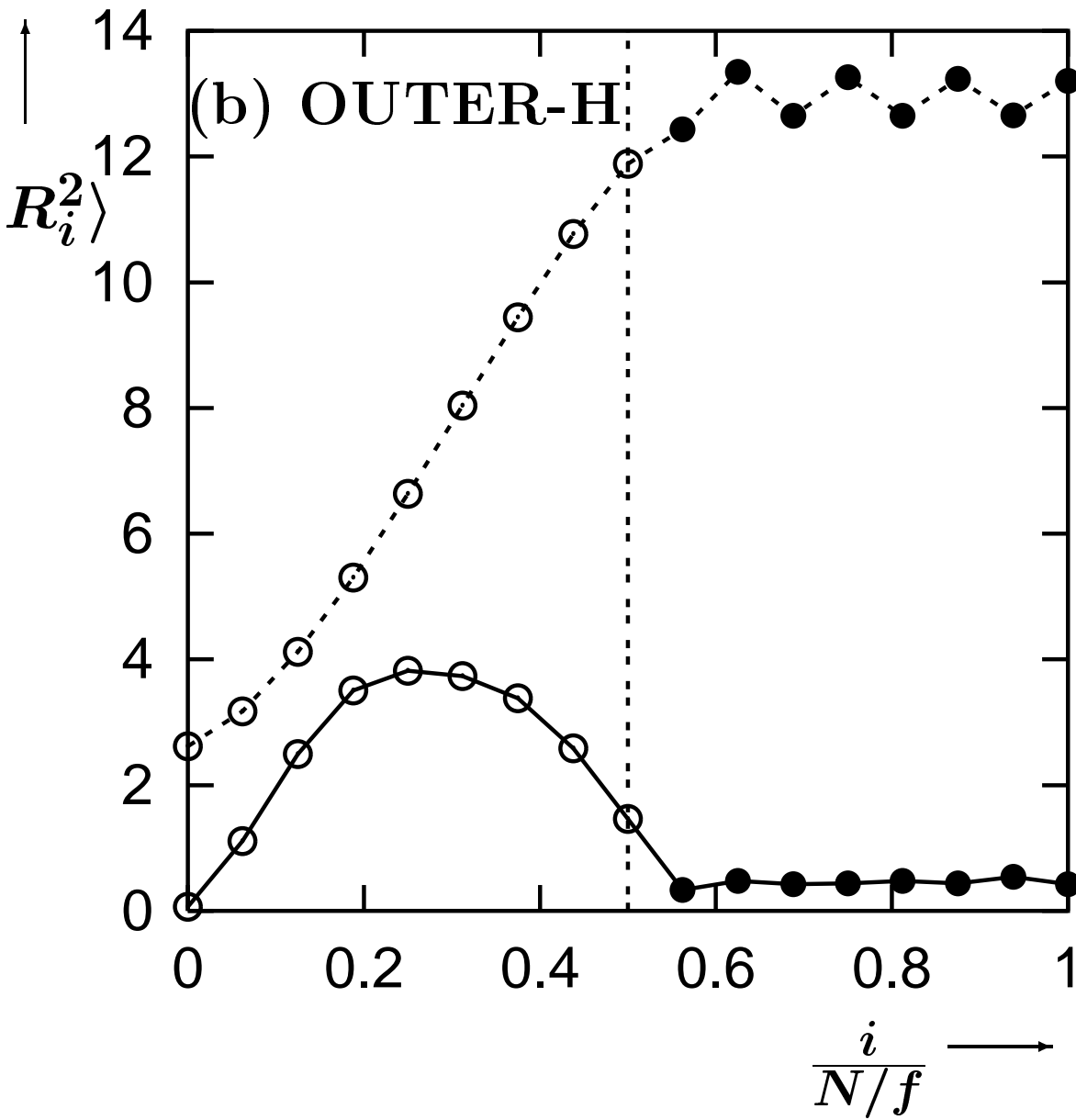


Fig. 3b

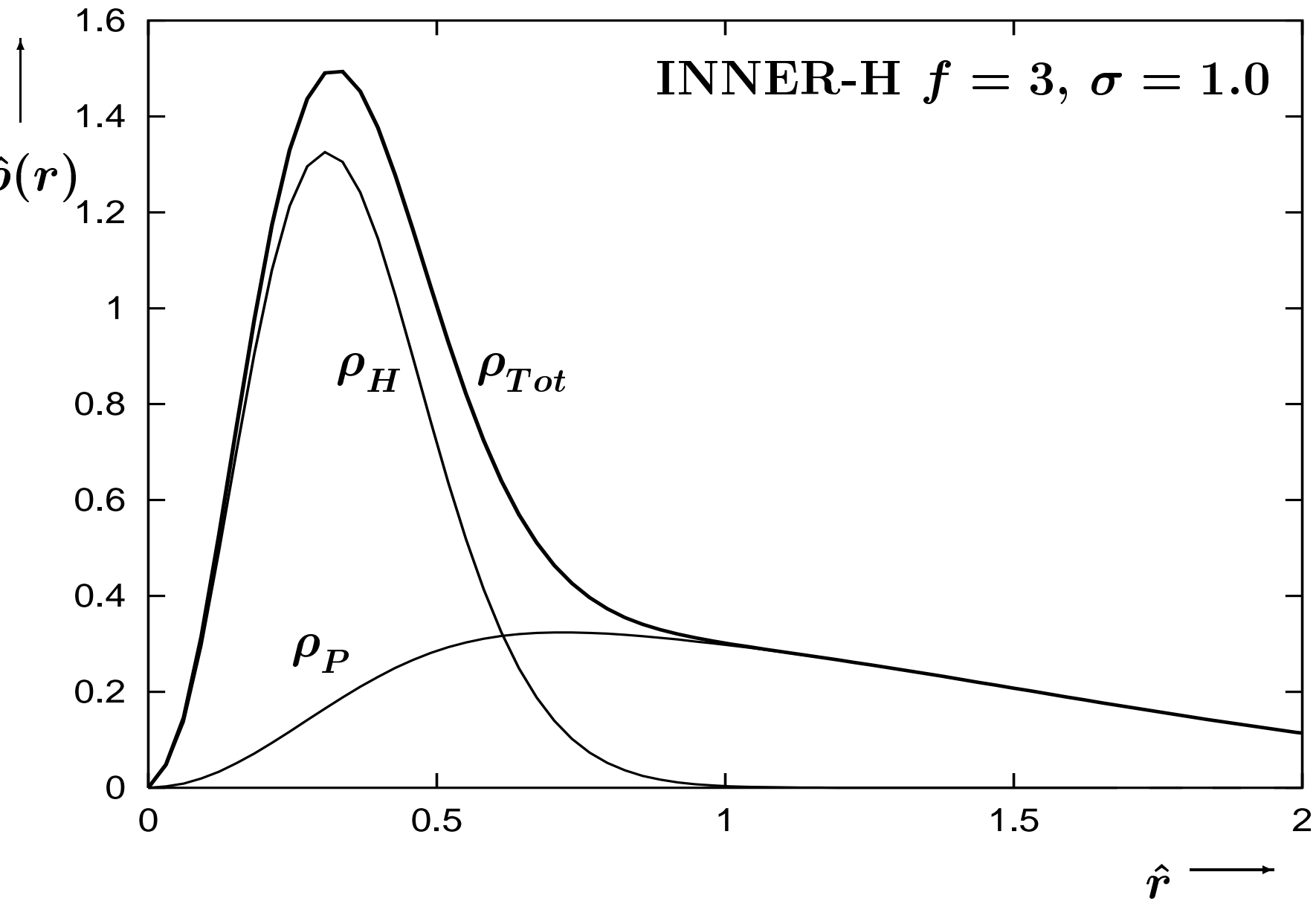


Fig. 4

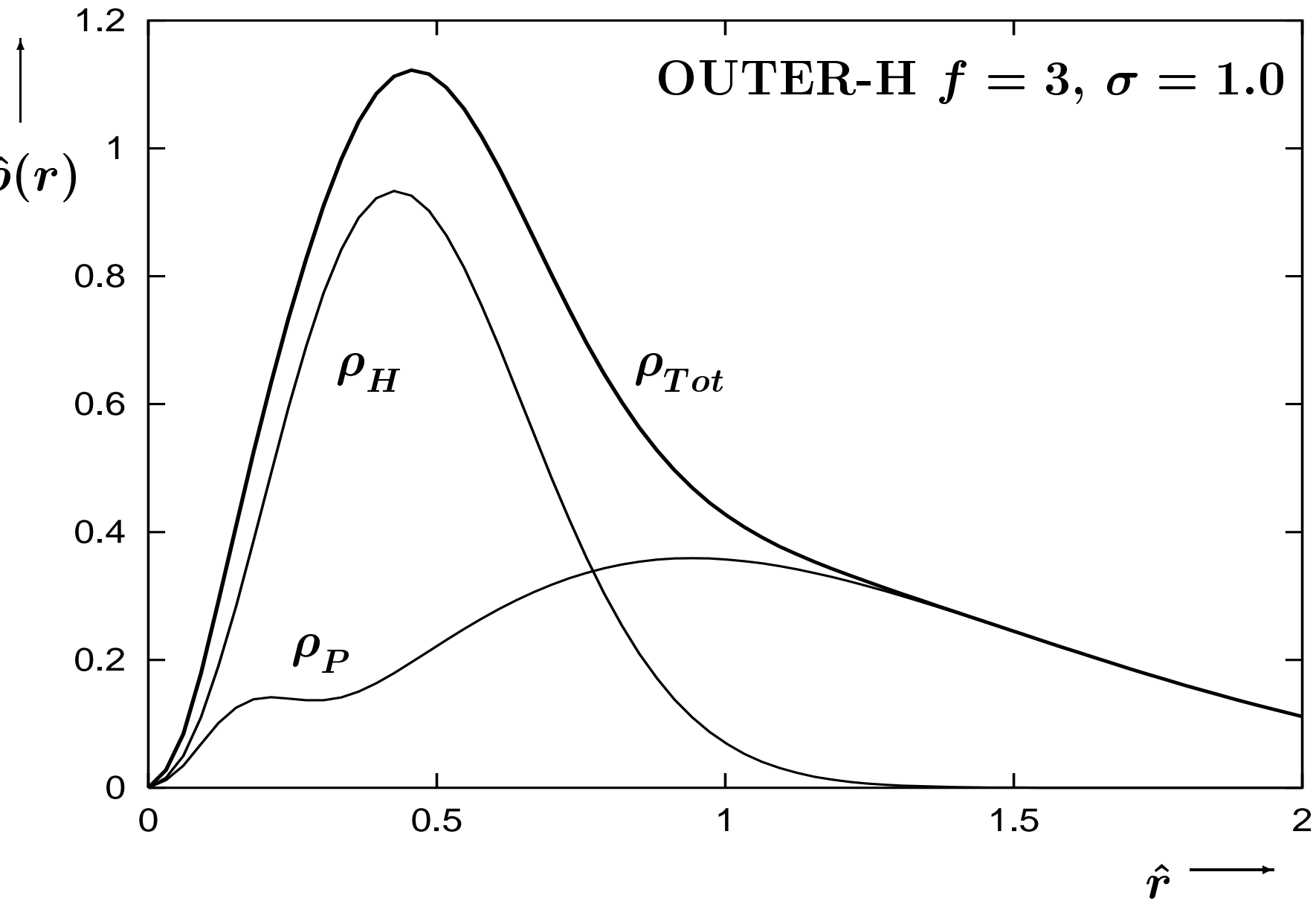


Fig. 5

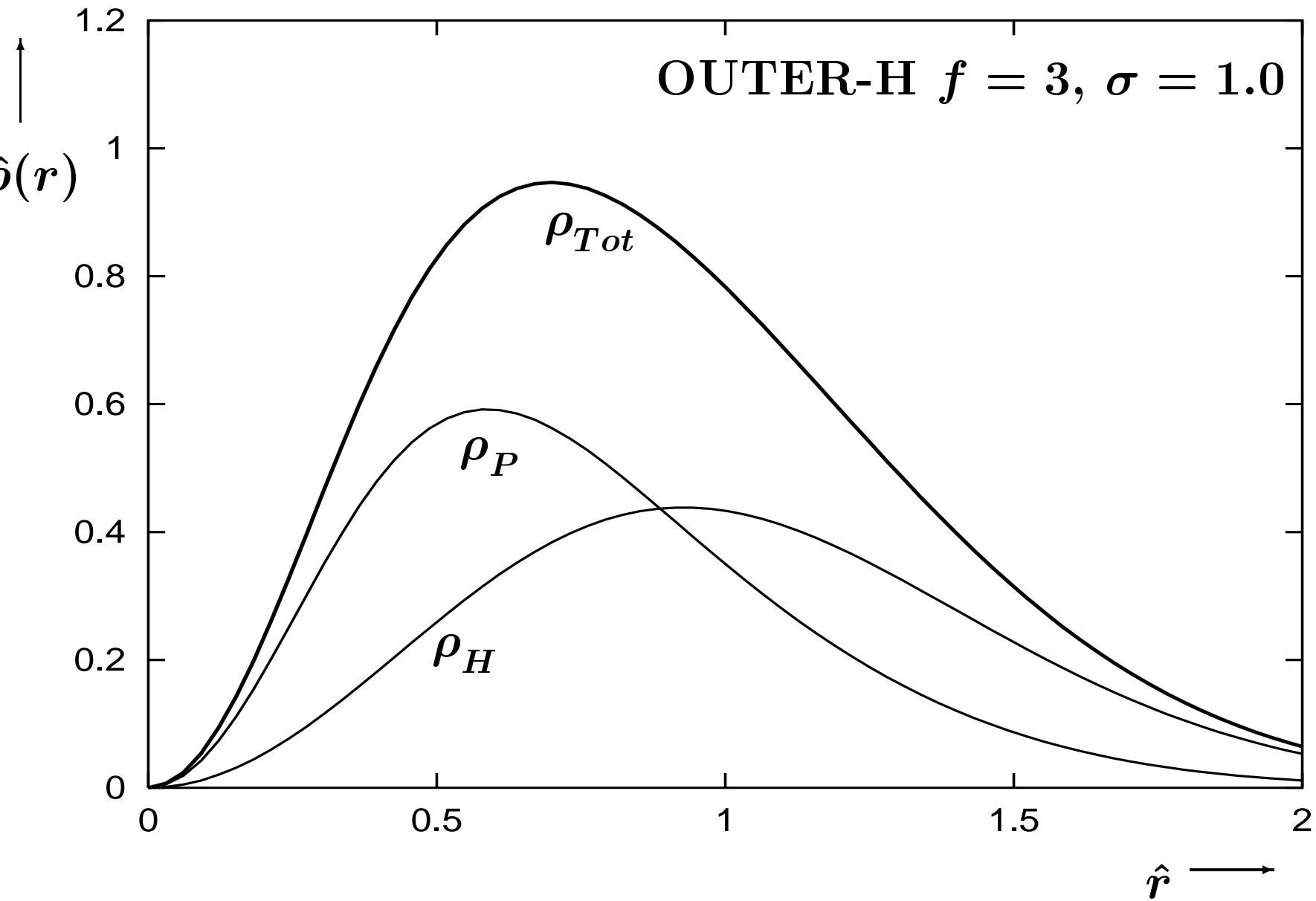


Fig. 6

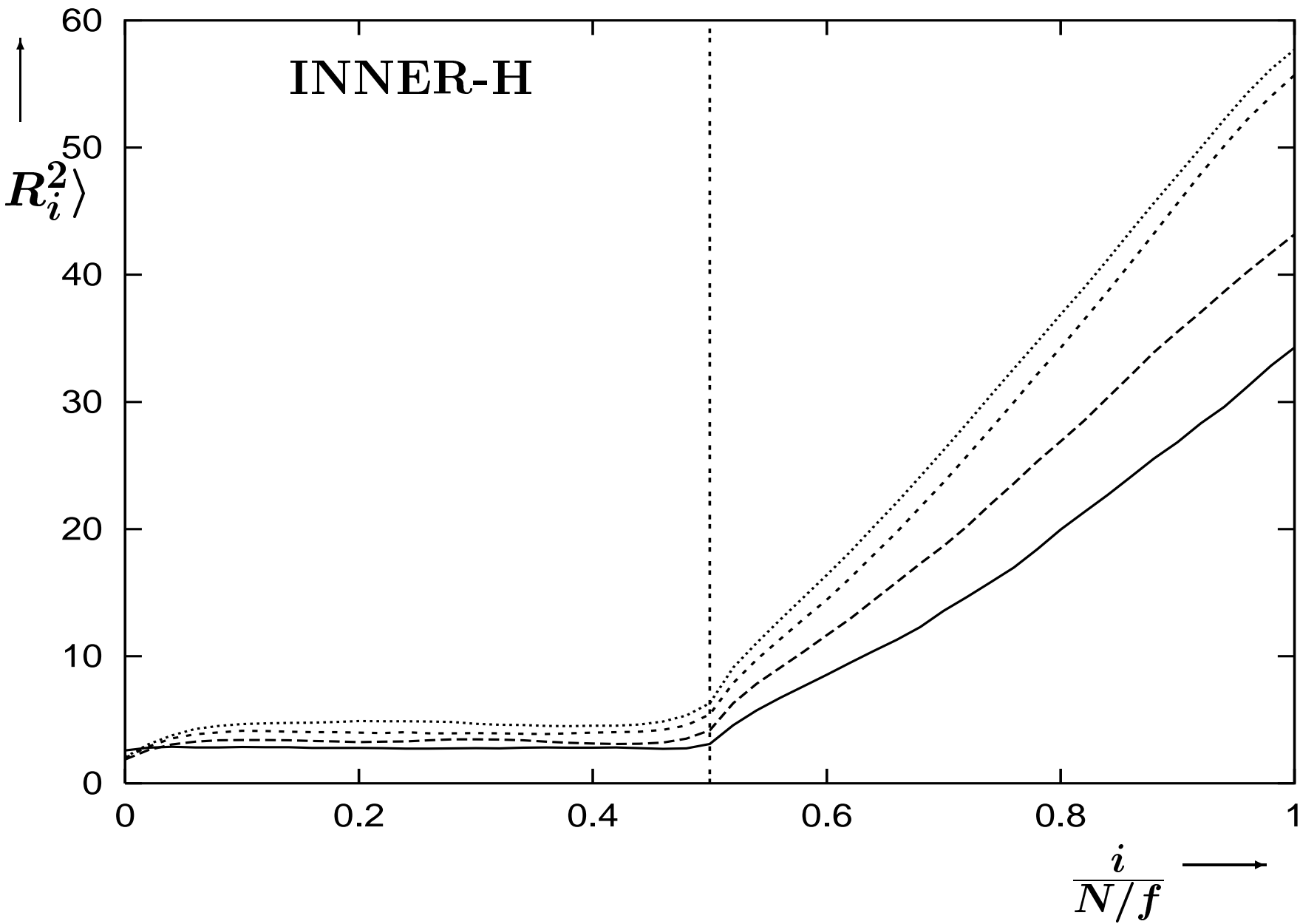


Fig. 8

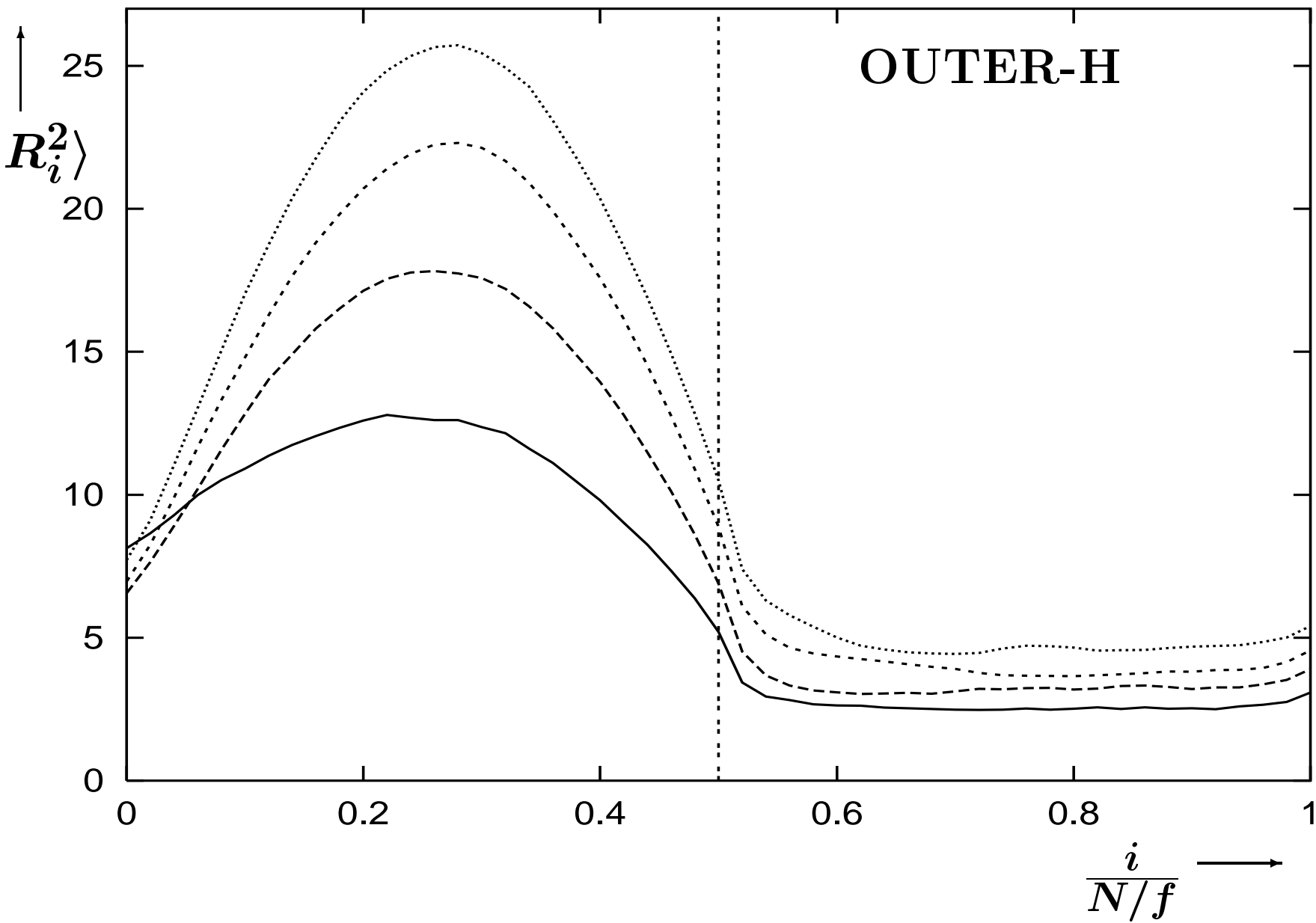


Fig. 11

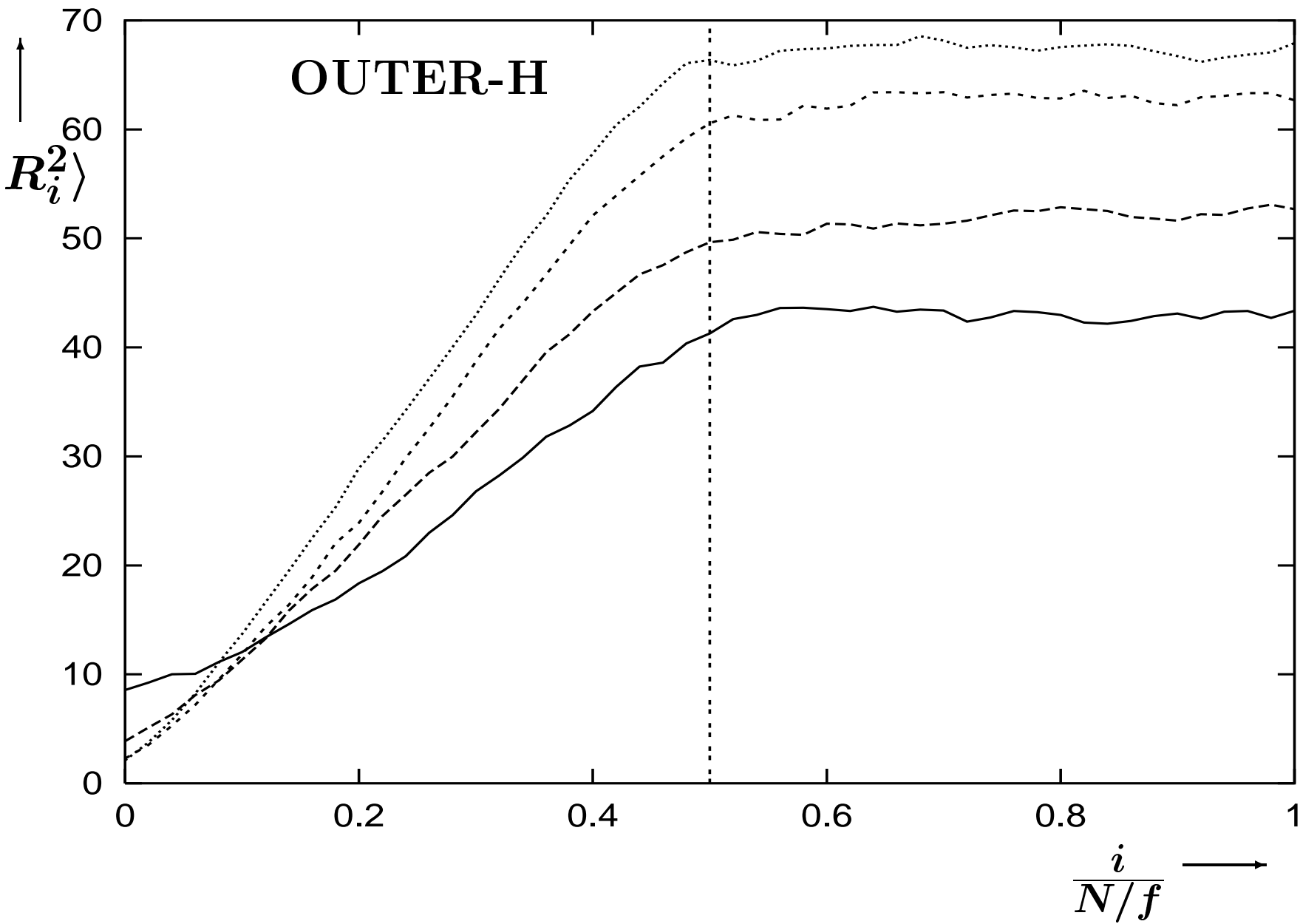


Fig. 14

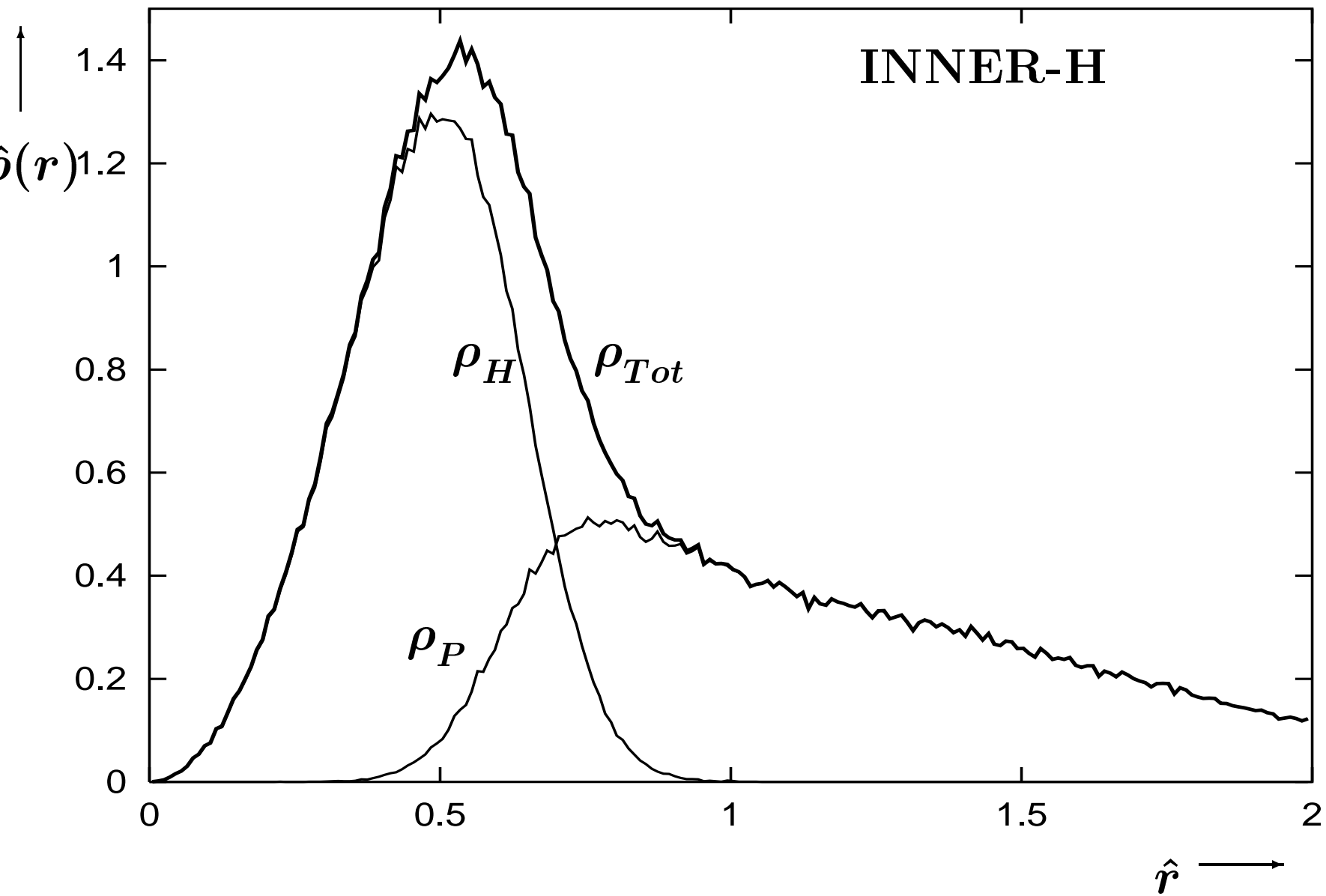


Fig. 9

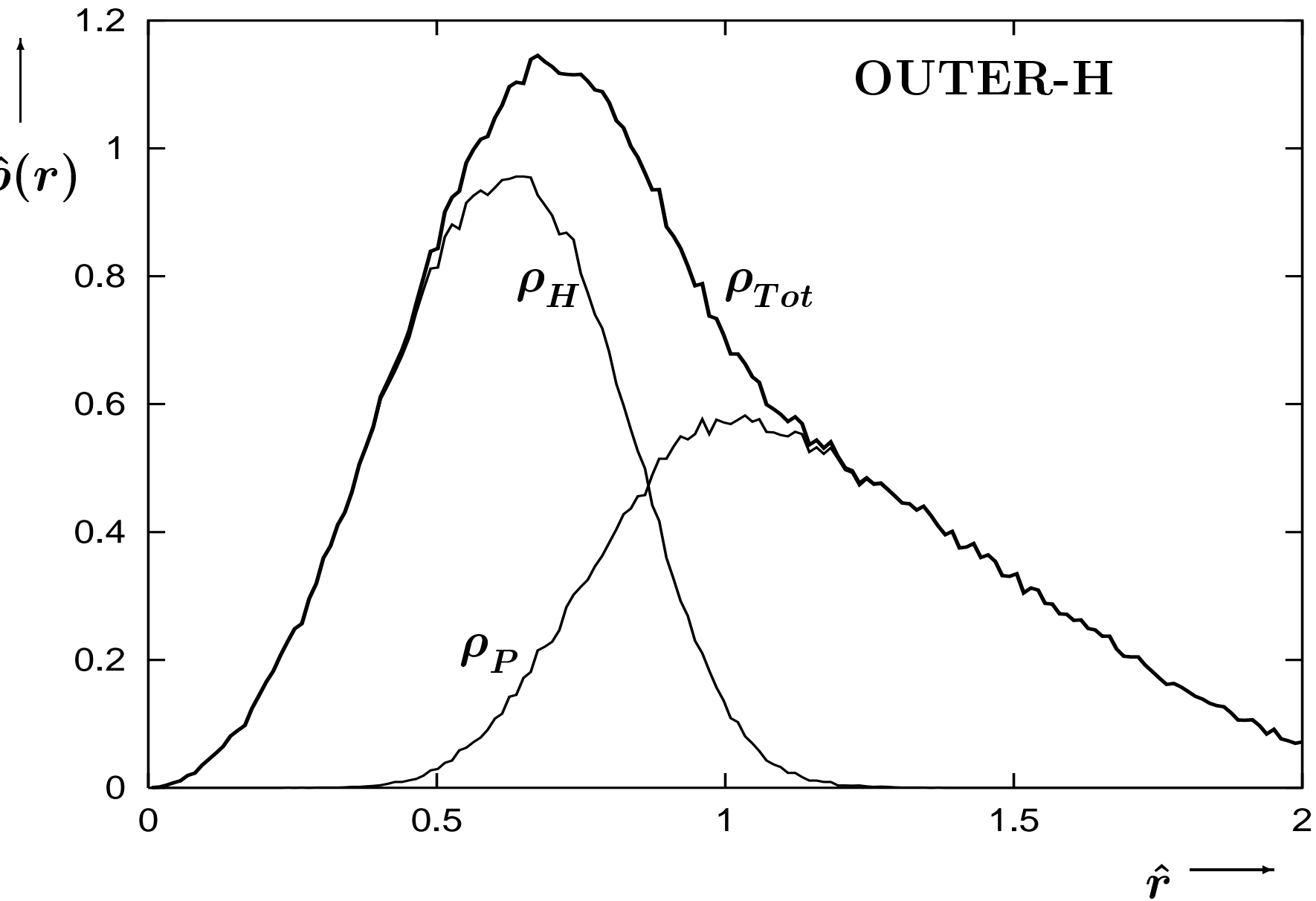


Fig. 12

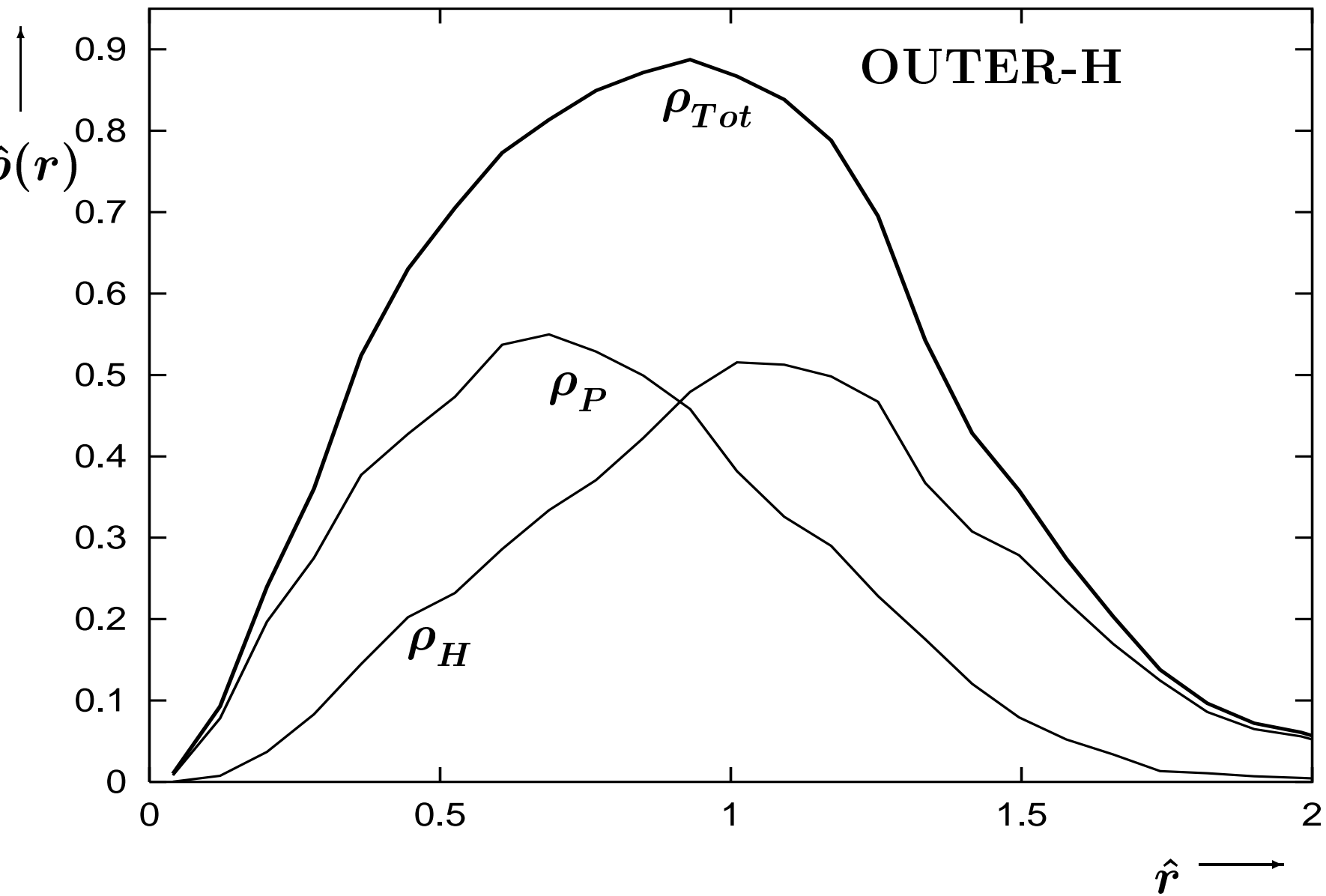


Fig. 15

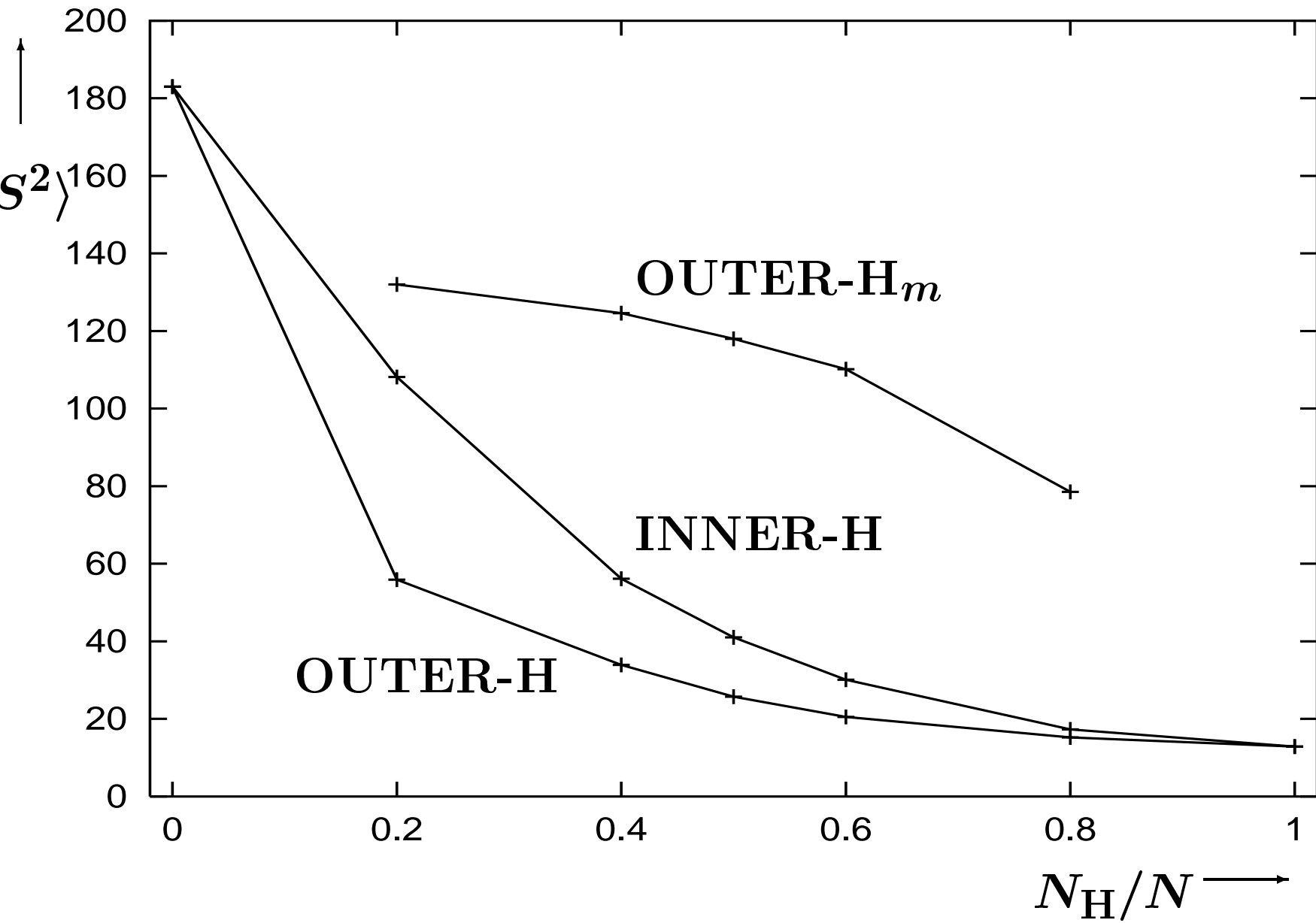


Fig. 16

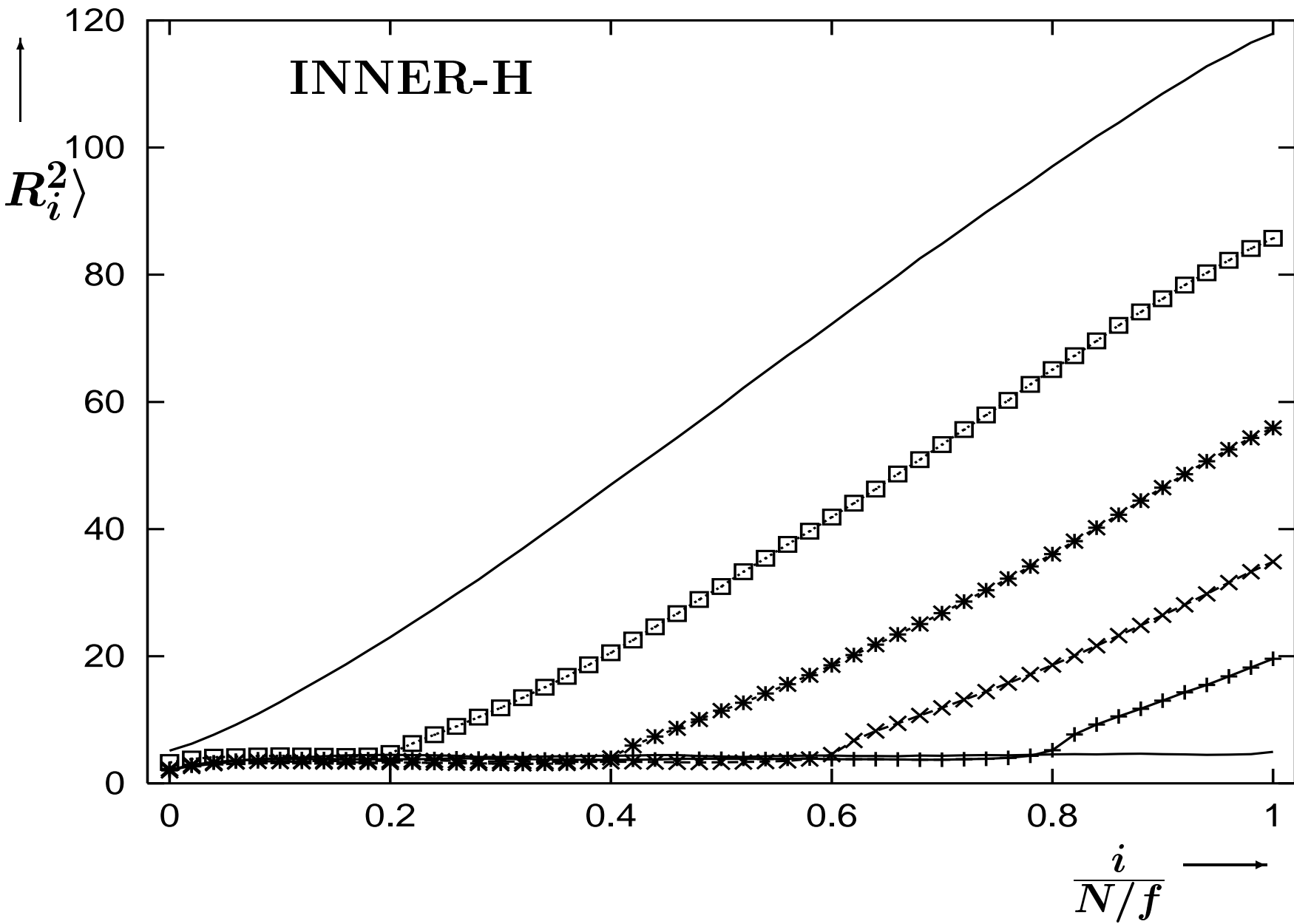


Fig. 17

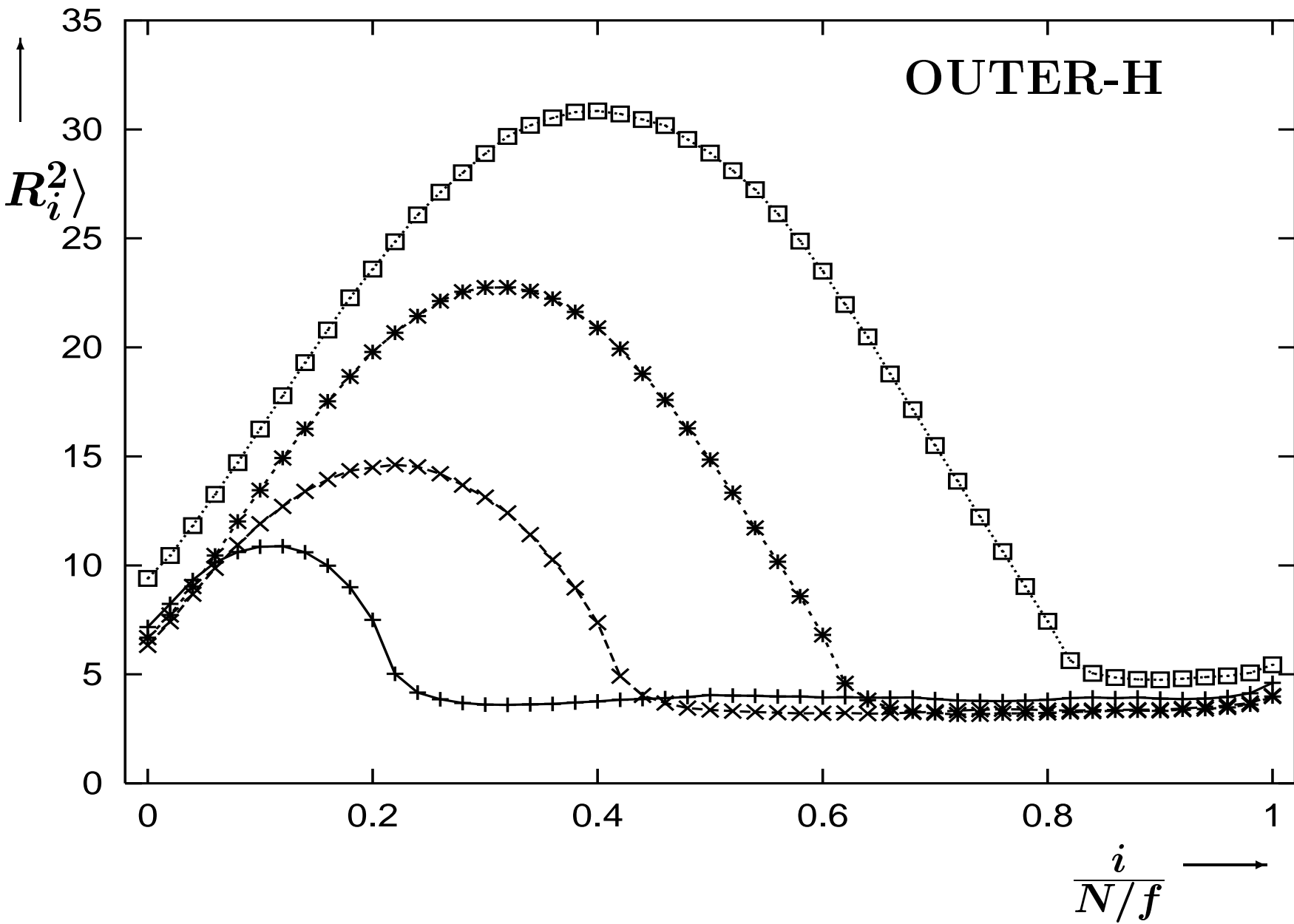


Fig. 18

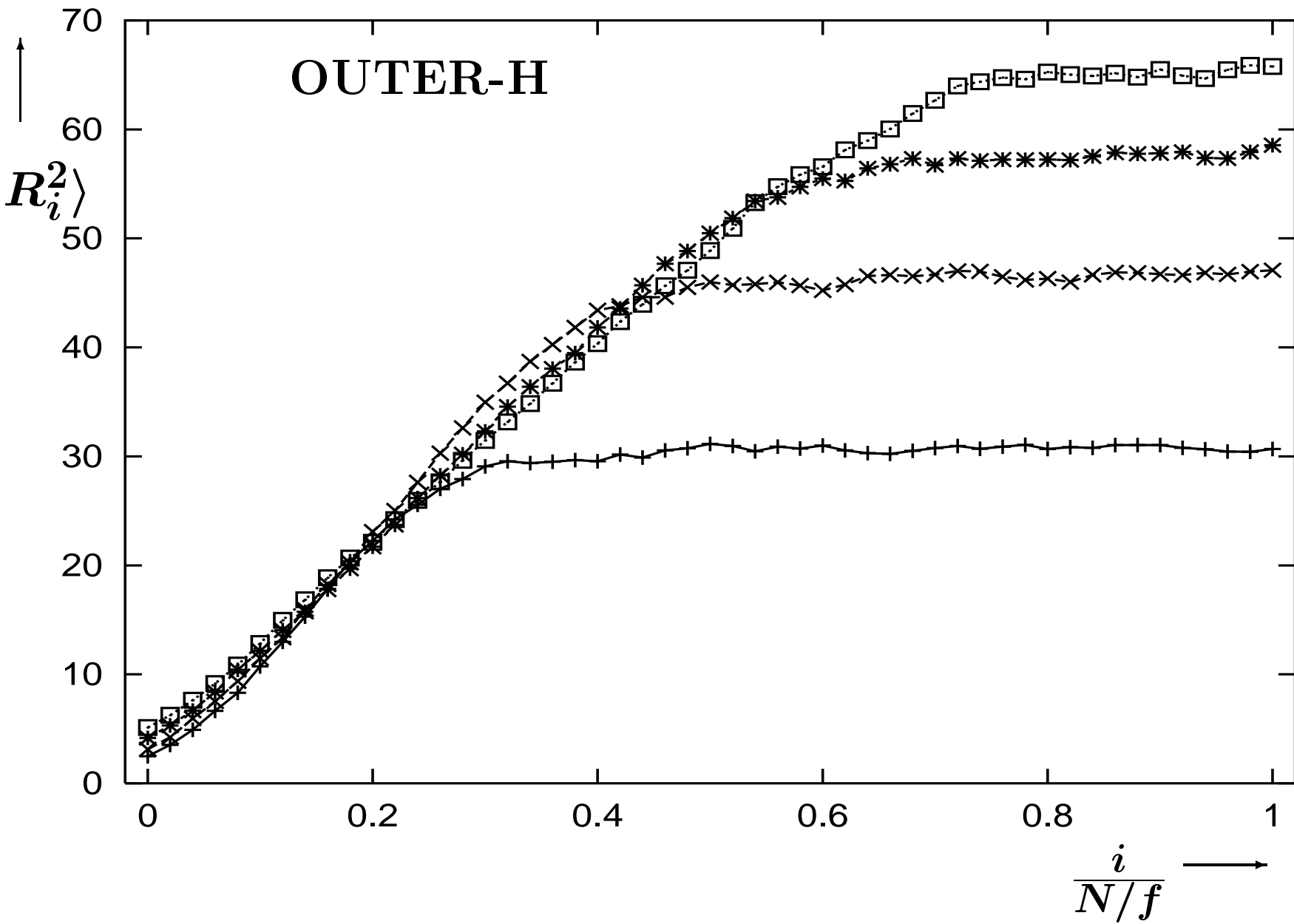


Fig. 19

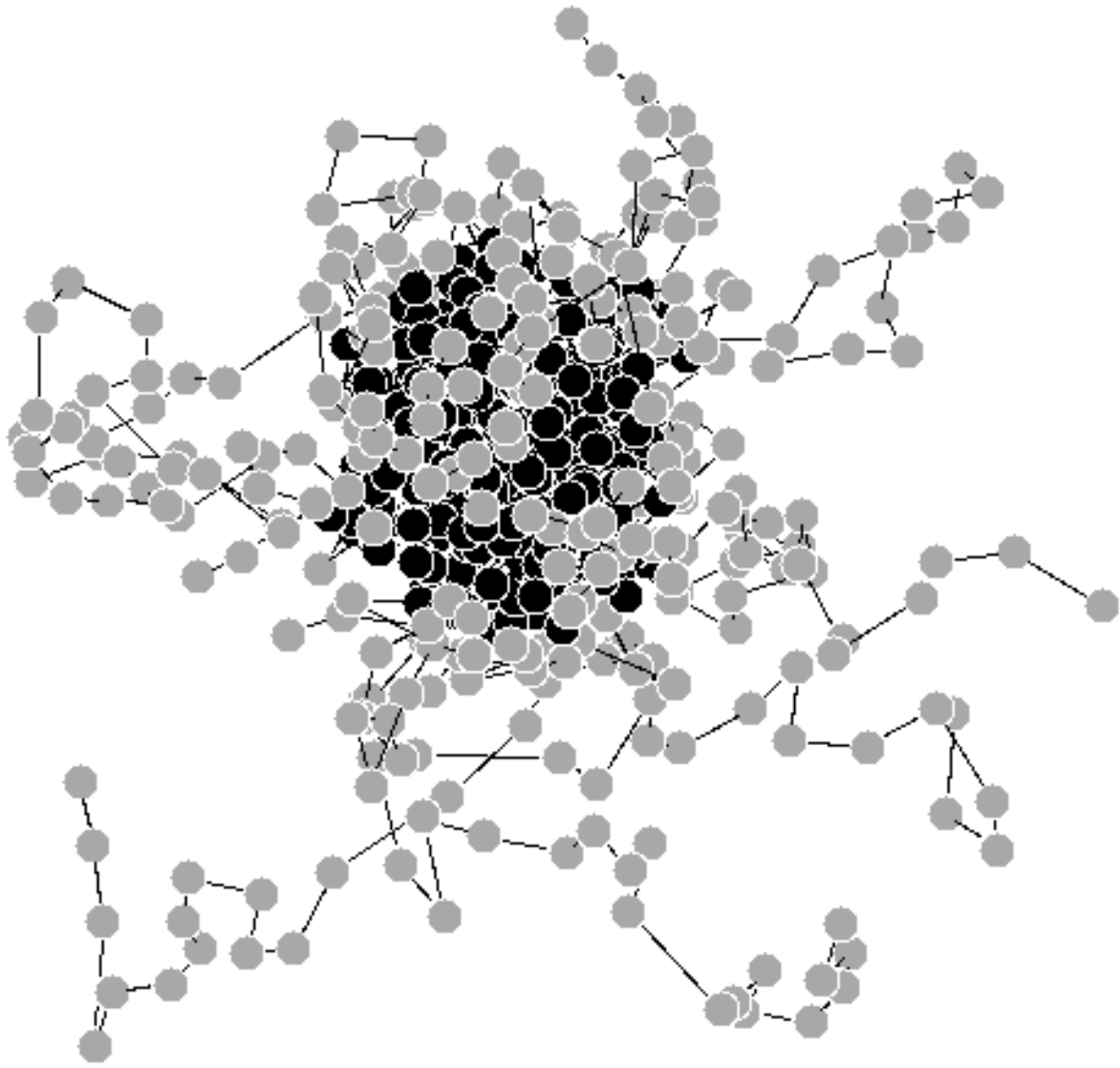


Fig. 7

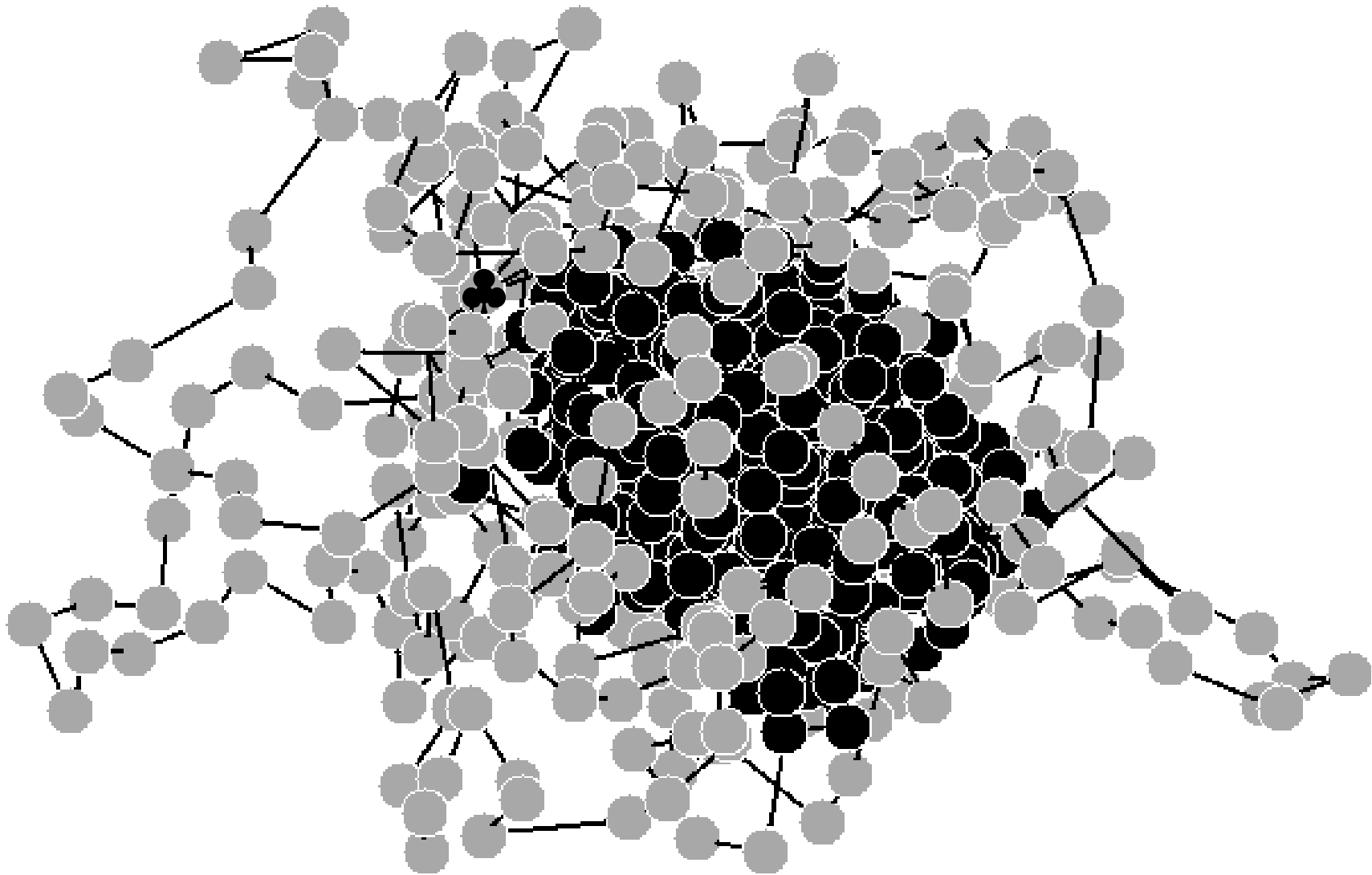


Fig. 10

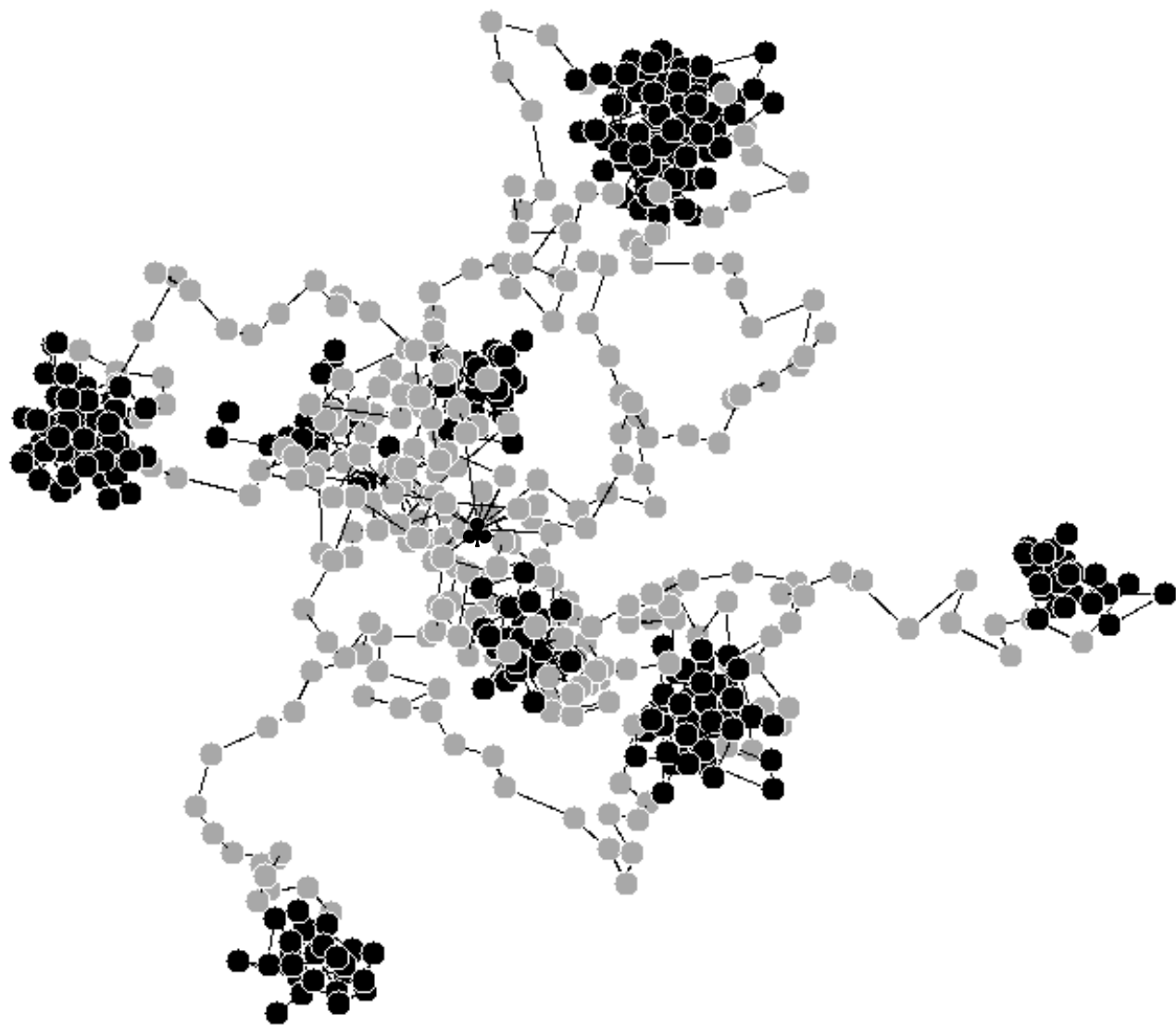


Fig. 13